Numerical investigation of cold-formed steel channels with edge-stiffened and unstiffened elongated web holes under shear

Dinesh Lakshmanan Chandramohan [a], Krishanu Roy [a]*, Zhiyuan Fang[a]*, Beulah Gnana Ananthi. G[b], James B.P. Lim[a,c]

[a] School of Engineering, The University of Waikato, New Zealand

[b] Division of Structural Engineering, College of Engineering Guindy campus, Anna University, India

[c] Department of Civil and Environmental Engineering, The University of Auckland, New Zealand

*Corresponding authors: Krishanu Roy, Zhiyuan Fang

Abstract

Over the past decade, cold-formed steel (CFS) channel sections having edge-stiffened circular web holes have been developed in New Zealand. Such edge-stiffened holes increase the strength of the CFS channel sections, compared to an equivalent section having unstiffened web holes, while still allowing full building service integration. In the case of shear, previous research has found that the use of edge-stiffened web holes significantly improves the shear strength of such channel sections. However, no studies are available in the literature investigating the shear strength of CFS channel sections with edge-stiffened elongated web holes. The issue is addressed herein. Non-linear finite element (FE) analyses are used to investigate the shear strength of CFS channel sections with a shear span aspect ratio of 2.0. The FE models were validated against the experimental test results of sections having unstiffened elongated web holes and edge-stiffened circular web holes; good agreement in terms of the load-displacement curves and failure behaviour was shown. Using the validated FE models, a parametric study was conducted, comprising 2,124 finite element analyses (FEA) results. The parametric results were then compared to the design predictions of the American Iron and Steel Institute (AISI 2016), and Australia/New Zealand Standards (AS/NZS 2018) and Wanniarchchi et al. (2017) for unstiffened elongated web holes,

showing that the design predictions are unconservative in comparison results. Moreover, the direct strength method (DSM) approach of Pham et al. (2020a and 2023) provides conservative results for channels with unstiffened elongated web holes. It was also found that the design equations proposed by Chen et al. (2018) for edge-stiffened circular web holes were unconservative in predicting the shear strength of channels having edge-stiffened elongated web holes. Therefore, design equations in the form of a shear reduction factor and a modified DSM approach for CFS channel sections having unstiffened and edge-stiffened elongated web holes were proposed. Finally, a reliability analysis was carried out to ensure that the proposed equations are reliable to predict the shear strength of CFS channel sections with edge-stiffened and unstiffened web holes.

Keywords: Elongated web holes; Edge-stiffened web holes; Shear strength; Cold-formed steel; Finite element analysis; Direct strength method

1. Introduction

Cold-formed steel (CFS) channel sections often require holes in the webs in order to allow services to be integrated within the floors. The presence of web holes in such sections influences shear behaviour and considerably reduces shear strength [1, 2].

Over the last decade, a new generation of CFS channel sections having edge-stiffened circular web holes has been developed and are now widely used in New Zealand (see Fig. 1). Experimental tests on such sections have been reported in the literature considering their failure behaviour in shear [3, 4], compression [5-7], bending [8-10] and web crippling [11, 12]. Design recommendations for each of these load cases were also proposed [3-4,6-8,10-11].

However, in some cases, it is necessary for elongated web holes to be used, in order for larger services to be accommodated (see Fig. 2a). As with the circular web holes, these elongated web holes can be edge-stiffened. Fig. 2b shows the parameters adopted in this paper to describe an

elongated web hole. No previous research has been reported on their shear strength and behaviour of these channel sections with elongated edge-stiffened web holes. Furthermore, the available design standards of the American Iron and Steel Institute (AISI) [13] and the Australian and New Zealand Standards (AS/NZS) [14] do not provide shear design equations for CFS channel sections having edge-stiffened web holes. Therefore, in this study, the shear behaviour of CFS channel sections having edge-stiffened elongated web holes was investigated and new design equations were proposed.

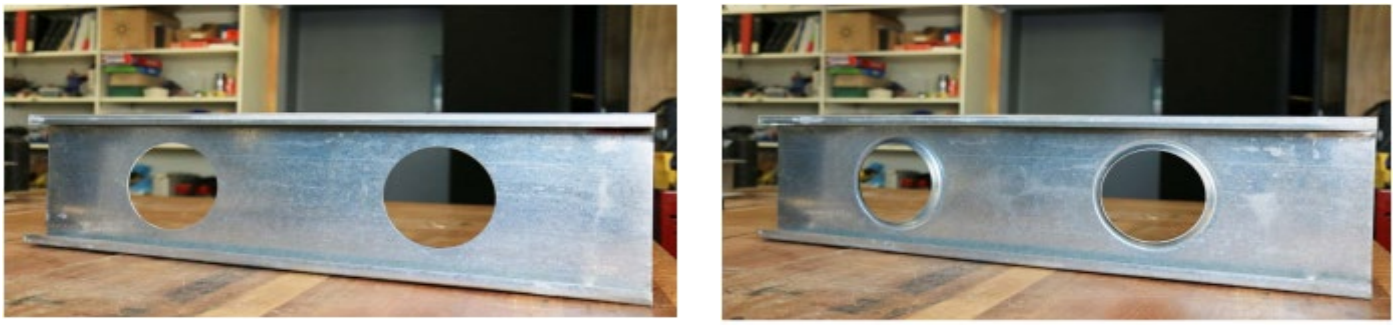

(a) Unstiffened web holes (b) Edge-stiffened web holes

Fig. 1 CFS channel sections with circular web holes [3]

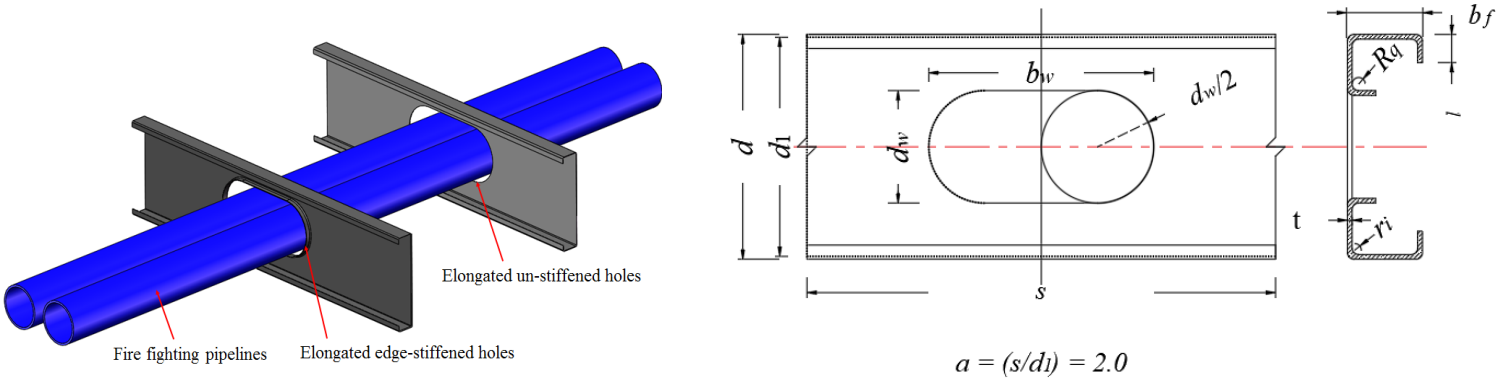

(a) Elongated web holes for building services (b) The details of elongated web holes

Fig. 2 Application and details of elongated web holes

In terms of CFS channel sections with unstiffened circular web holes, many studies were reported in the literature that investigate their shear strength and behaviour. Eiler et al. [15] investigated the shear behaviour of CFS channel sections having unstiffened circular web holes

and proposed a shear reduction factor (q_s) for such channels, which is currently being used by the AISI [13] and AS/NZ [14]. Keerthan and Mahendran [16, 17] studied both experimentally and numerically the effect of unstiffened circular web holes on the shear behaviour of CFS channel sections with shear span aspect ratios of 1.0 and 1.5. They also compared the experimental and numerical results to AISI [13] and AS/NZ [14] design predictions, which showed conservative results for shear strength of CFS channels having unstiffened circular web holes. Therefore, modified design equations in the form of shear reduction factor were proposed for such channels. Similarly, Chandramohan et al. [18] proposed modified shear reduction factor and DSM based equations for doubly symmetric hollow flange beams with web holes. Recently, Pham et al. [1, 2, 19-21] studied the shear behaviour of CFS channel sections having unstiffened circular web holes and proposed a new direct strength method (DSM) based approach for calculating the shear strength of such channels. Additionally, other studies have investigated the effect of CFS channel sections with unstiffened circular web holes under different loading conditions [22-26].

For CFS channel sections with edge-stiffened circular web holes, limited research is available in the literature investigating its shear strength. Chen et al. [3] performed an experimental and numerical investigation on the shear behaviour of CFS channels having edge-stiffened circular web holes. It was found that the test results of channels having edge-stiffened web holes showed an average 14.5% higher shear strength than the shear strength of channels having unstiffened web holes. Similarly, Kanthasamy et al. [4] investigated the shear strength and behaviour of CFS doubly symmetric hollow flange beams with edge-stiffened circular web holes. Their study found that the presence of edge-stiffened web holes significantly improves the shear strength, and they recommended the optimum edge-stiffener length of 15 mm for such beams irrespective of web

hole sizes. In addition, some studies investigated the effect of edge-stiffened circular web holes on CFS channel sections under compression [5-7], bending [8-10] and web crippling [11, 12].

For CFS channel sections with unstiffened elongated web holes, few studies are available in the literature that investigated its shear strength and behaviour. Pham et al. [1, 2] conducted an experimental and numerical investigation on the shear strength of CFS channel sections having unstiffened elongated web holes considering the effect of different web hole depths and lengths. Based on the experimental and numerical results, a new DSM design equations incorporating Vierendeel mechanism approach were proposed to determine the shear strength of CFS channels having unstiffened elongated web holes [1, 2]. The proposed DSM design equation is quite complex to implement into the current design standards such as in AISI [13] and AS/NZ [14]. Therefore, Pham et al. [19, 27] provided alternative DSM based equations for calculating the shear strength of CFS channels with unstiffened elongated web holes by means of cubic fit to Vierendeel model equations [1, 2]. Similarly, Pham et al. [1, 28] also investigated the shear behaviour of CFS channel sections with unstiffened rectangular and square web holes. They found that the shear strengths of CFS sections with rectangular web holes are lower than those with elongated web holes due to the larger area of rectangular web holes compared to elongated web holes of the same dimension [1]. Furthermore, Shan et al. [29] performed an experimental investigation on the CFS channel sections having unstiffened elongated web holes under shear. On the other hand, Wanniarachchi et al. [30] conducted numerical studies on the shear strength of CFS channel sections having unstiffened elliptical web holes. It was found that the current design standards are unconservative in predicting the shear strength of such channels. Therefore, modified design equations based on the shear reduction factor were proposed, and a suitable DSM based equation was also developed. Besides, in terms of columns, some studies on CFS channels having

unstiffened elongated web holes [31-35] were investigated under axial compression, which showed different buckling failures depending on their slenderness.

For edge-stiffened elongated web holes, Wei et al. [36] numerically investigated the web crippling capacity of CFS channel sections with edge-stiffened elongated web holes under interior-two-flange (ITF) loading condition. However, no research was found in the literature investigating the shear strength and behaviour of CFS channel sections having edge-stiffened elongated web holes. The issue is addressed in this paper.

This paper presents a numerical study using non-linear elastic-plastic finite element analysis (FEA) to investigate the effect of unstiffened and edge-stiffened elongated web holes on the shear strength of CFS channel sections with a shear span aspect ratio (a) of 2.0. The shear span aspect ratio is the ratio of shear span to the depth of web (s/d_1). The developed finite element (FE) models were validated against the experimental results reported by Pham et al. [1, 27] and Chen et al. [3] on unstiffened elongated web holes and circular edge-stiffened web holes, respectively. From the FEA results, design equations in the form of a shear reduction factor and a modified DSM based approach were proposed to determine the shear strength of CFS channel sections considering the effects of unstiffened and edge-stiffened elongated web holes. Finally, the reliability of all the proposed design methods was assessed by means of statistical analyses, showing their suitability for incorporation into future revisions of international design codes for CFS structures.

2. Summary of experimental investigations by Pham et al. [1, 37] and Chen et al. [3]

The experimental test results reported by Pham et al. [1, 37] focused on CFS channel sections with plain webs and unstiffened elongated web holes subjected to shear loading (a = 2.0), were used in this paper for the validation purpose. While Chen et al. [3] provided FE modeling techniques for the shear behaviour of CFS channel sections with edge-stiffened web holes, their

investigation only considered circular web holes, disregarding elongated web holes. Therefore, the current study utilized the test results and modeling techniques from Pham et al. [1, 37] (Table 1) and Chen et al. [3] (Table 2) to develop FE models for CFS channel sections with edge-stiffened elongated web holes, aiming to examine their shear strength.

3. Numerical investigation

3.1 General

Nonlinear elasto-plastic FE models were developed using ABAQUS software [38] to simulate the shear behaviour of CFS channel sections with plain webs, unstiffened elongated web holes and edge-stiffened elongated web holes. In the FE modeling, the centerline cross-section dimensions as well as the initial geometric imperfections for CFS channel sections were considered. The following subsections provide a detailed description of the modeling techniques.

3.2 Material properties

The material properties of CFS steel grades G300 and G450 with nominal yield strengths (f_y) of 300 MPa and 450 MPa, respectively, were considered in this study. In the current study, the material models proposed by Gardner and Yun [39] and Rossi et al. [40] were used to determine the stress-strain behaviour for CFS sections in flat and corner regions, respectively. Gardner and Yun [39] proposed stress-strain models based on the previous research done on CFS sections to determine the material behaviour considering various material strengths, sections and manufacturing processes. They also recommended equations by Rossi et al. [40] to determine the material model of the corner regions. Plastic deformation in the corner regions during the manufacturing process causes corner strength enhancement [40]. Fig. 3 shows the material stress-stress curves for the yield strengths of 300 MPa and 450 MPa. As per the ABAQUS manual

148 [38], the engineering stress-strain curves were converted into a true stress-strain curves by using
149 the following equations:

150 $$\sigma_{true} = \sigma\,(1+\varepsilon) \quad (1)$$

151 $$\varepsilon_{true} = ln\,(1+\varepsilon) - \frac{\sigma_{true}}{E} \quad (2)$$

152 Where σ_{true} and ε_{true} are the true stress and strain, respectively, while σ and ε are the
153 engineering stress and strain, and E represents the elastic modulus.

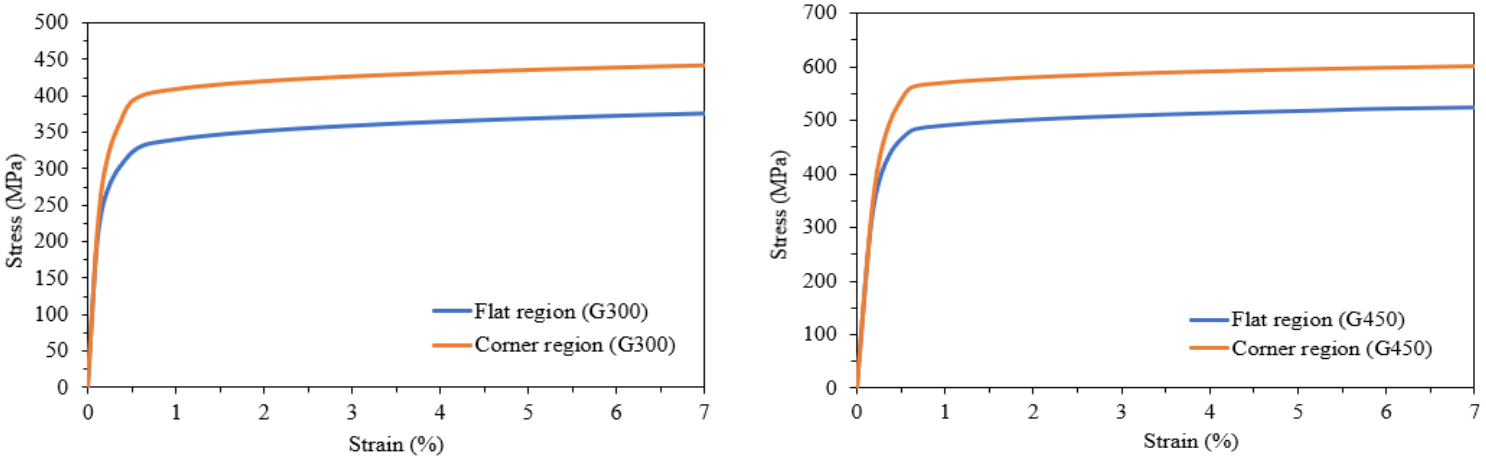

(a) For CFS steel grade G300 (b) For CFS steel grade G450

Fig. 3 The material stress-stress curves for a yield strengths of 300 MPa and 450 MPa [39, 40]

154 *3.3 Meshing*

155 S4R shell elements were used to model the CFS channel sections, while C3D4 solid elements
156 were chosen to model the loading plates. Based on the results of mesh sensitivity analysis, the
157 mesh size used for the loading plates and channel sections was determined to be 10 mm × 10 mm
158 and 5 mm × 5 mm, respectively. Finer mesh size was adopted for the areas (a) between the web
159 and flange region (b) between the flange and lip region and (c) between the edge-stiffener and the
160 web region (see Fig. 4).

3.4 Boundary and loading conditions

To simulate the dual actuator test rig used by Pham et al. [1, 37], the shear end plate (see Fig.5) was considered as a fixed support where the translational and rotational movements of x, y and z directions were restrained. To load the CFS channel sections, the reference points were set at the top of two loading plates (1 and 2), where all the translation movements except y-direction and the rotational movement of z-direction were restrained at the reference points (see Fig.5). The vertical displacement-controlled loading was applied at the reference points. In the FE model, the surface-to-surface interaction with "hard' contact property was employed in order to avoid the penetration between the CFS channel and the loading plate. Fig. 5 illustrates the boundary conditions of section C240-T2-D0.5-B2.5-Q0.12-R2. Similar modeling techniques were used by Pham et al. [2, 37] for investigating the shear strength of CFS channel sections having unstiffened elongated web holes and plain webs with a shear span aspect ratio of 2.0.

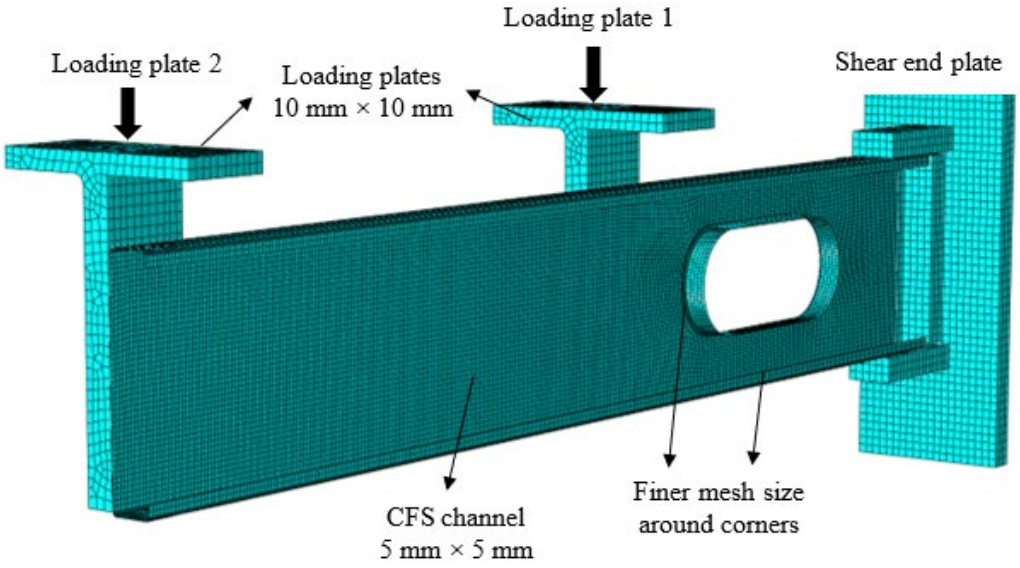

Fig. 4 FE meshing of specimen C240-T2-D0.5-B2.5-Q0.12-R2

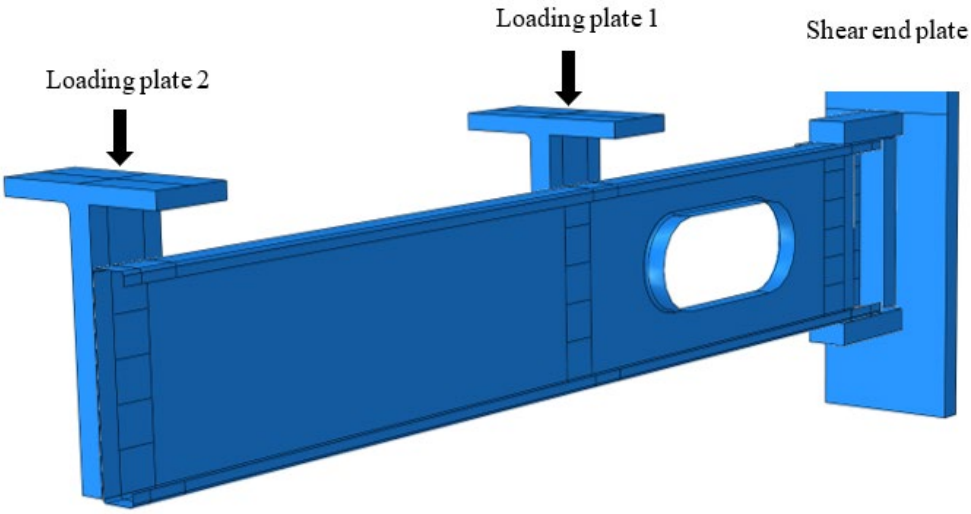

Fig. 5 Applied boundary conditions on specimen C240-T2-D0.5-B2.5-Q0.12-R2

3.5. Geometrical imperfections

In the FE modeling, initial geometrical imperfections were considered. The magnitude of local imperfections was taken as 0.64 t for the CFS channel sections [2]. The ABAQUS library's *IMPERFECTION option was used to model the imperfect initial geometries of CFS channel sections in the current study. The FE models included the critical buckling mode obtained from the eigenvalue buckling analysis as the imperfect geometries.

3.6 Validation of the FE model

A comparison of the test results (V_{EXP}) of Pham et al. [1, 37] and Chen et al. [3] with the FEA results (V_{FEA}) was summarized in Tables 1 and 2. The mean and coefficient of variation (COV) values of the V_{EXP} / V_{FEA} ratio were 1.05 and 0.09 for unstiffened elongated web holes and plain webs, respectively, and 1.07 and 0.03 for edge-stiffened circular web holes, respectively. Figs. 6 and 8 depicted the failure behaviour observed in both the experimental tests and the FEA. The developed FE model exhibited similar failure behaviour to the test results for both unstiffened elongated and edge-stiffened circular web holes. Shear strength versus displacement curves were

plotted in Figs. 7 and 9, showing a good agreement between the FEA and test results. Overall, the FE model developed in this paper showed a good correlation with the test results.

Table 1 Comparison of FEA results against test results of Pham et al. [1, 37] for the shear strength of plain webs and unstiffened elongated web holes

Section dimensions ($d \times b_f \times l$)	Test series number	Aspect ratio a	Hole depth d_w	Hole length b_w	Hole depth ratio d_w/d_1	Test V_{EXP}	FEA V_{FEA}	V_{EXP}/V_{FEA}
(mm×mm×mm)			(mm)	(mm)		(kN)	(kN)	
200×65×15	Test-1	2.0	-	-	-	47.50	46.08	1.03
	Test-2	2.0	-	-	-	47.80	46.08	1.03
200×65×15	Test-1	2.0	40	80	0.21	41.39	40.50	1.02
	Test-2	2.0	40	80	0.21	41.44	40.50	1.02
200×65×15	Test-1	2.0	40	120	0.21	35.90	36.82	0.97
	Test-2	2.0	40	120	0.21	35.97	36.82	0.98
200×65×15	Test-1	2.0	80	160	0.42	24.21	24.49	0.98
	Test-2	2.0	80	160	0.42	24.09	24.49	0.98
200×65×15	Test-1	2.0	120	240	0.63	11.82	10.71	1.10
	Test-2	2.0	120	240	0.63	11.65	10.71	1.08
200×65×15	Test-1	2.0	120	360	0.63	7.59	6.18	1.23
	Test-2	2.0	120	360	0.63	7.62	6.18	1.23
							Mean	1.05
							COV	0.09

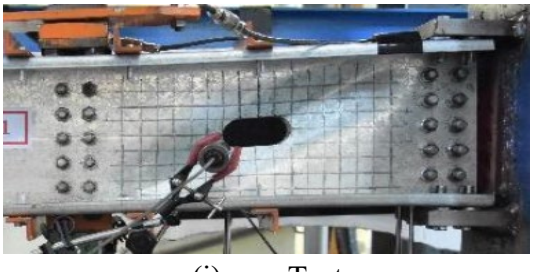

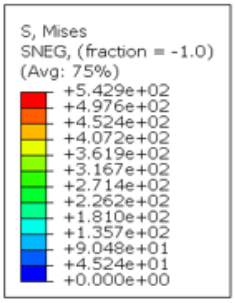

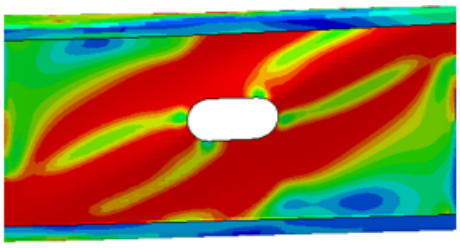

(i) Test (ii) FEA

(a) Hole size 40×80

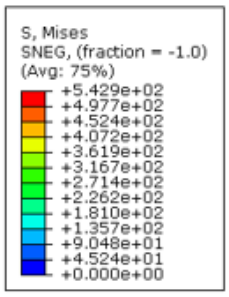

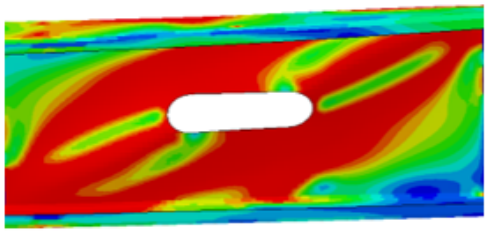

(i) Test (ii) FEA

(b) Hole size 40×120

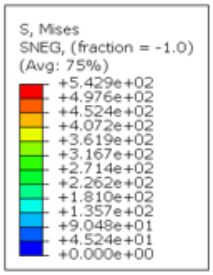

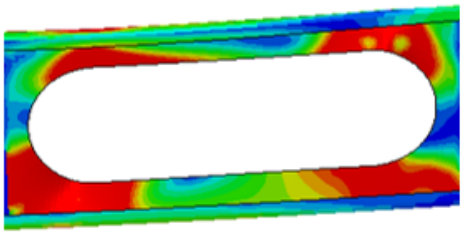

(i) Test (ii) FEA

(c) Hole size 120×360

Fig. 6 Comparison of test [1] and FEA failure behaviour for unstiffened elongated web holes

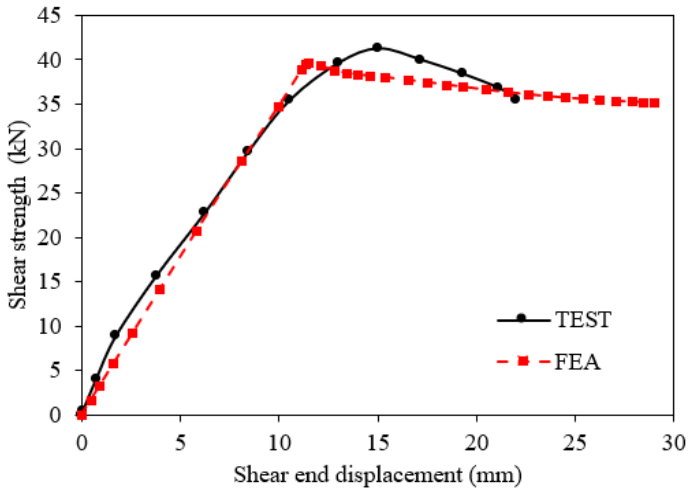

Fig. 7 Comparison of load-displacement curves for the specimen with hole size 40×80 [1]

Table 2 Comparison of FEA results against test results of Chen et al. [3] for the shear strength of edge-stiffened circular web holes

Section dimensions						Shear strength		
Web depth d	Web thickness t_w	Aspect ratio a	Hole depth d_{wh}	Hole depth ratio d_{wh}/d_1	Stiffener length q	Test V_{EXP}	FEA V_{FEA}	V_{EXP}/V_{FEA}
(mm)	(mm)		(mm)		(mm)	(kN)	(kN)	
237.3	1.86	1.0	96.5	0.41	13	31.7	33.0	1.04
238.3	1.85	1.5	93.5	0.39	13	28.7	30.4	1.06
235.5	1.87	1.0	148.9	0.63	13	41.0	45.3	1.10
237.3	1.85	1.5	147.5	0.62	13	35.2	38.6	1.09
							Mean	1.07
							COV	0.03

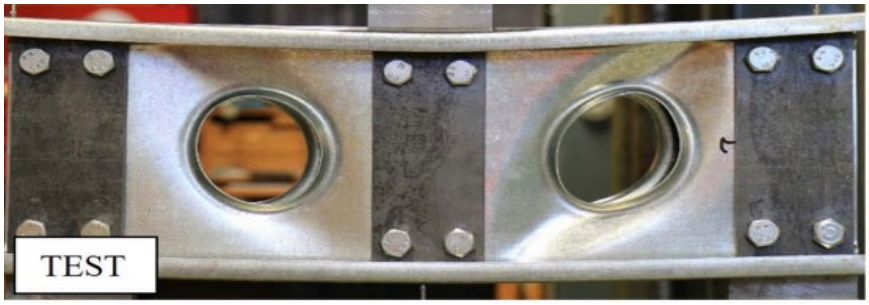

(a) Test

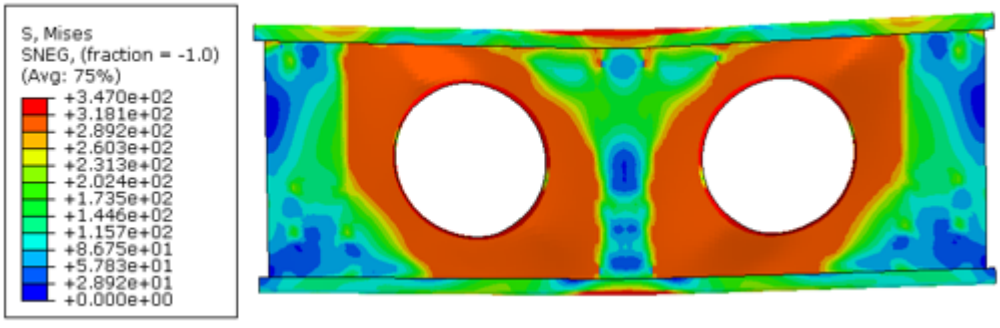

(b) FEA

Fig. 8 Comparison of shear failure behaviour for the specimen 240-A1.0-D140-EH-FU [3]

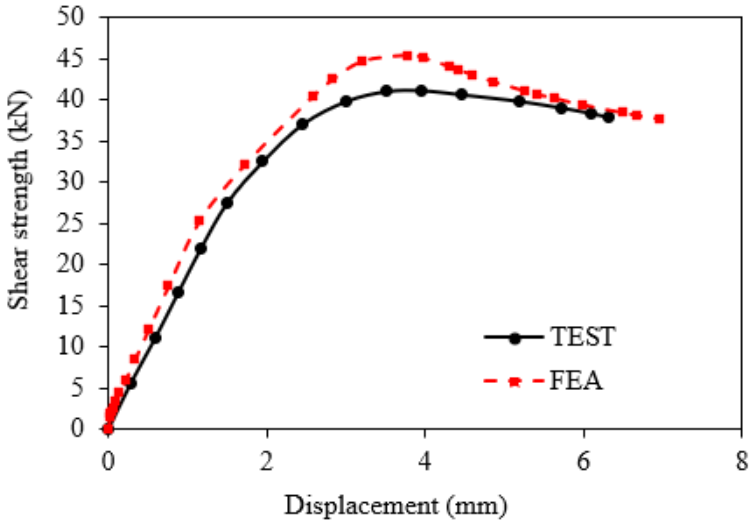

Fig. 9 Comparison of load-displacement curves for the specimen 240-A1.0-D140-EH-FU [3]

4. Parametric study

4.1 parametric design and section labelling

Using the same FE modeling techniques described in Section 3, a parametric study comprising the results of 2,124 FEA was conducted on CFS channel sections having plain webs, unstiffened and edge-stiffened elongated web holes. In the current study, CFS channel sections (a = 2.0) having two different section depths (d) of 240 mm and 290 mm (see Fig. 10), thicknesses (t) varying from 1 mm to 2 mm, and yield strengths (f_y) of 300 MPa and 450 MPa were considered. To investigate the effect of specimens with elongated web holes (see Fig. 2b), the following parameters were varied: the ratio of hole depth to web depth (d_w/d_1) from 0.1 to 0.7; the ratio of hole length to hole depth (b_w/d_w) from 2 to 3; the ratio of stiffener length to web depth (q/d_1) from 0.04 to 0.12; and the inner bent radius between the web flat and stiffener (R_q) from 2 to 6 mm. Due to the length of the hole exceeding the shear span length, the ratio of hole depth to web depth (d_w/d_1) was restricted to 0.5 for sections having a b_w/d_w ratio of 3.

The specimens used for the parametric study were labelled such that the web depth, thickness, web hole depth ratio, web hole length ratio, stiffener length ratio, and inner bent radius between the web and stiffener were defined. Fig. 11 illustrates the labelling of the investigated channel sections in the parametric study. For example, the label "C290-T1-D0.3-B2-Q0.02-R2" can be explained as given below.

- "C290" indicates the depth of the section in millimeters i.e., d = 290 mm.
- "T1" defines the thickness of the section in millimeters i.e., t = 1 mm.
- "D0.3" refers to the hole depth to web depth ratio (d_w/d_1) i.e., d_w/d_1 = 0.3.
- "B2" refers to the hole length to hole depth ratio (b_w/d_w) i.e., b_w/d_w = 2.
- "Q0.04" defines the stiffener length to hole depth ratio (q/d_1) i.e., q/d_1 = 0.04.
- "R2" refers to the inner bent radius between the flat portion of the web to the stiffener (R_q) i.e., R_q = 2.

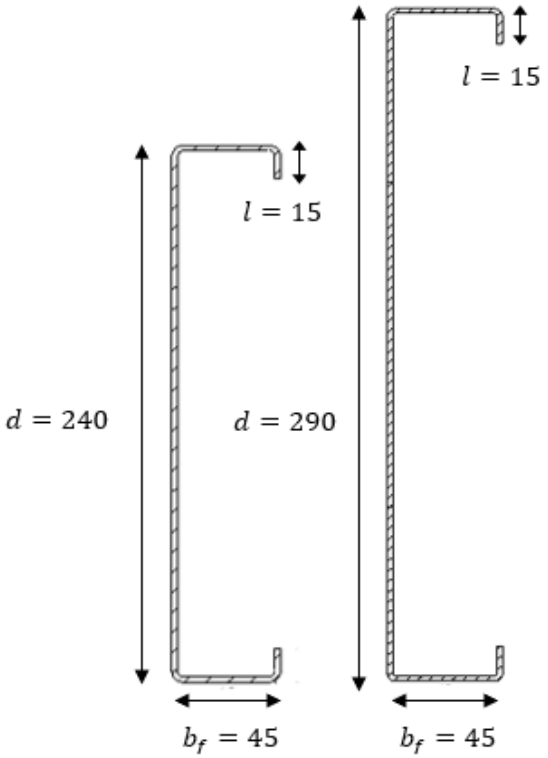

Fig. 10 Nominal cross-sections of the CFS channel sections considered for the parametric study

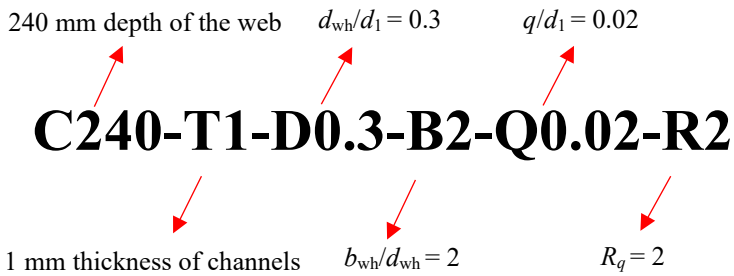

Fig. 11 Specimen labelling used in the parametric study

4.2. Result and discussion

The shear strengths of CFS channel sections having plain webs, unstiffened, and edge-stiffened elongated web holes obtained from the FEA are presented in Table 3. From the results of parametric study, the qualitative effects of d_w/d_1, b_w/d_w, and q/d_1 on the shear reduction factor for unstiffened and edge-stiffened elongated web holes were investigated in the following sub-

sections. For edge-stiffened web holes, it was found that the q_s factor decreased by an average of 1.5% only when the R_q value increased from 2 to 6, indicating that the R_q has a negligible effect.

4.2.1 Effects of d_w/d_1 on q_s factor for unstiffened elongated web holes

Table 3 and Fig. 12 show the effects of the d_w/d_1 ratio on q_s factor for CFS channel sections having unstiffened elongated web holes. From the results of parametric study, it was found that the q_s factor decreased by 87% on average, when the d_w/d_1 ratio was varied from 0.1 to 0.7 for sections with unstiffened web holes.

4.2.2 Effects of b_w/d_w on q_s factor for unstiffened elongated web holes

The effect of the b_w/d_w ratio on q_s factor for CFS channels having unstiffened elongated web holes is shown in Table 3 and Fig. 13. It can be seen that a decreasing trend in q_s factor was observed when the b_w/d_w ratio was increased. From the results, it was found that the q_s factor decreased by an average of 18% when the b_w/d_w ratio was increased from 2 to 3.

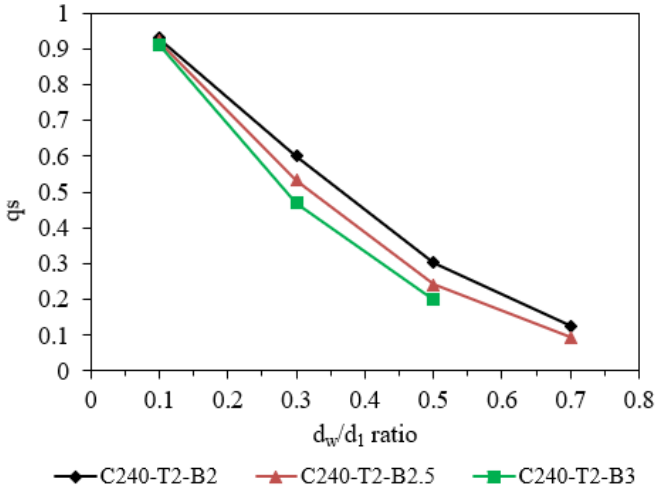

Fig. 12 Effect of d_w/d_1 ratio on q_s factor for CFS channel sections with unstiffened elongated web holes (f_y = 300 MPa)

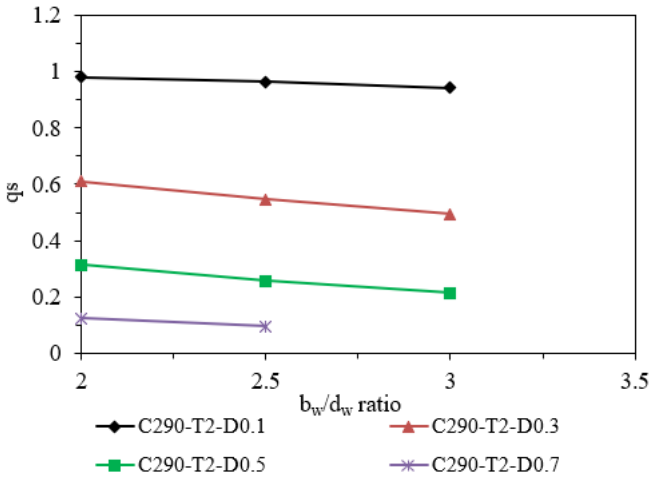

Fig. 13 Effect of b_w/d_w ratio on q_s factor for CFS channel sections with unstiffened elongated web holes (f_y = 450 MPa)

4.2.3 Effects of q/d_1 on q_s factor for edge-stiffened elongated web holes

Table 3 and Fig. 14 show the effects of the q/d_1 ratio on q_s factor for CFS channel sections having edge-stiffened elongated web holes. It can be seen from Fig. 12 that the ratio q/d_1 has a considerable effect on q_s factor. From the FEA, it was found that increasing the q/d_1 ratio from 0.04 to 0.12, increased the q_s factor by an average of 10%. Moreover, the CFS channel sections with edge-stiffened elongated web holes having a q/d_1 ratio from 0.04 to 0.12 showed an increase in the q_s factor by an average of 38% when compared to the sections with unstiffened elongated web holes.

4.2.4 Effects of d_w/d_1 on q_s factor for edge-stiffened elongated web holes

Table 3 and Fig. 15 show the effects of the d_w/d_1 ratio on q_s factor for CFS channel sections having edge-stiffened elongated web holes. From the results, it was found that the q_s factor decreased by 62% on average when the d_w/d_1 ratio was varied from 0.1 to 0.7 for edge-stiffened web holes. It is important to note that the d_w/d_1 ratio has a significant effect on the q_s factor.

4.2.5 Effects of b_w/d_w on q_s factor for edge-stiffened elongated web holes

The effect of the b_w/d_w ratio on q_s for channels having edge-stiffened elongated web holes is shown in Table 3 and Fig. 16. It can be seen that a decreasing trend in the q_s factor was observed when the b_w/d_w ratio increased. From the results, it was found that the q_s factor decreased by an average of 16% when the b_w/d_w ratio was increased from 2 to 3.

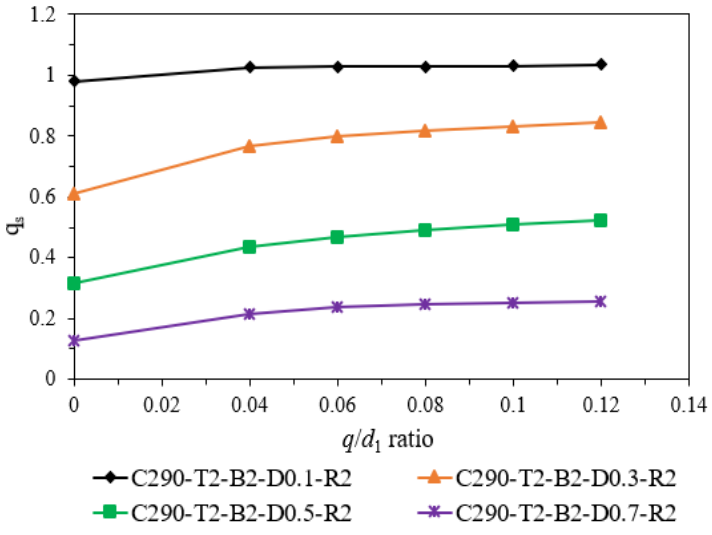

Fig. 14 Effect of q/d_1 ratio on q_s factor for CFS channel sections with edge-stiffened elongated web holes (f_y = 450 MPa)

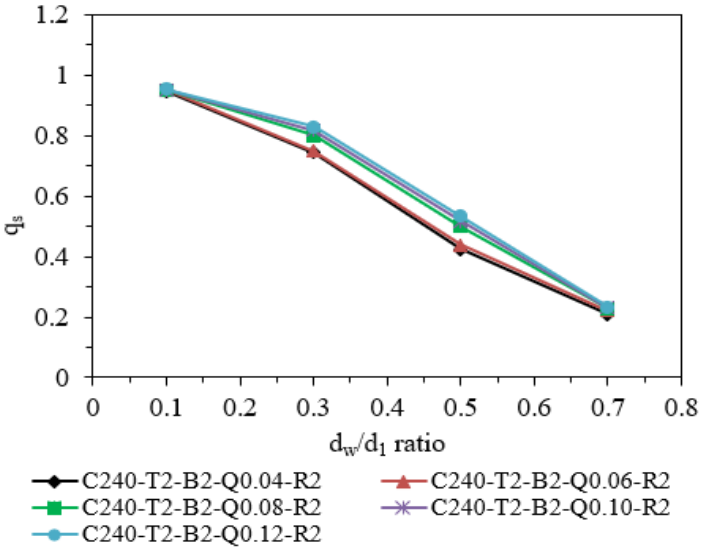

Fig. 15 Effect of d_w/d_1 ratio on q_s factor for CFS channel sections with edge-stiffened elongated web holes (f_y = 300 MPa)

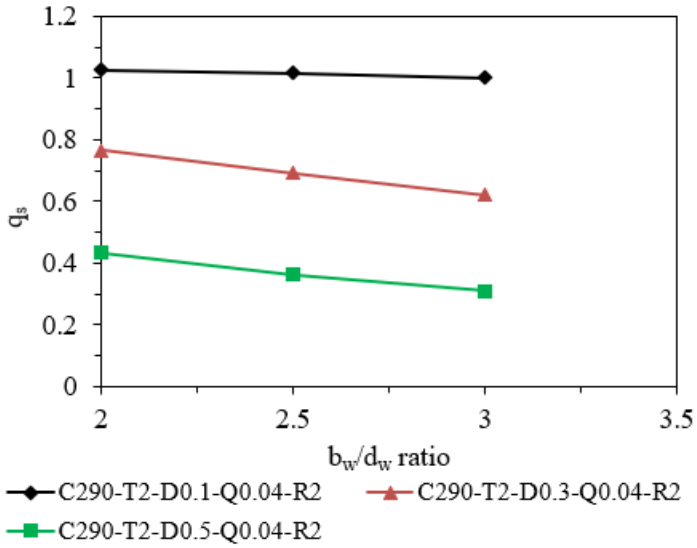

Fig. 16 Effect of b_w/d_w ratio on q_s factor for CFS channel sections with edge-stiffened elongated web holes (f_y = 450 MPa).

249

Table 3a Shear strength obtained from the parametric study for section C240 with yield strength (f_y) of 300 MPa

Specimen	Plain web	Unstiffened elongated web holes	Shear strength results of edge-stiffened elongated web holes from FEA, V_{FEA} (kN)														
			R_q=2					R_q=4					R_q=6				
			Q0.04	Q0.06	Q0.08	Q0.10	Q0.12	Q0.04	Q0.06	Q0.08	Q0.10	Q0.12	Q0.04	Q0.06	Q0.08	Q0.10	Q0.12
	(kN)	(kN)	(mm)	(mm)	(mm)	(mm)	(mm)	(mm)	(mm)	(mm)	(mm)	(mm)	(mm)	(mm)	(mm)	(mm)	(mm)
C240-T1.0-D0.1B2.0	20.86	19.78	20.17	20.26	20.35	20.39	20.51	20.15	20.21	20.30	20.34	20.45	20.12	20.18	20.23	20.30	20.36
C240-T1.0-D0.3B2.0	20.86	12.13	16.13	16.25	16.67	16.81	16.94	14.71	14.86	15.48	15.69	15.81	14.46	14.71	14.9	15.37	15.50
C240-T1.0-D0.5B2.0	20.86	6.43	8.12	8.28	9.28	9.58	9.70	8.10	8.26	9.14	9.41	9.63	8.07	8.24	8.63	9.26	9.47
C240-T1.0-D0.7B2.0	20.86	2.45	3.87	4.21	4.72	4.88	4.99	3.84	4.16	4.67	4.84	4.96	3.81	4.13	4.62	4.80	4.91
C240-T1.0-D0.1B2.5	20.86	19.23	19.77	19.84	19.88	19.90	19.95	19.71	19.75	19.56	19.86	19.90	19.68	19.70	18.89	19.76	19.88
C240-T1.0-D0.3B2.5	20.86	11.11	13.38	13.41	14.28	14.53	14.63	13.31	13.30	14.12	14.36	14.48	13.26	13.23	13.67	14.18	14.29
C240-T1.0-D0.5B2.5	20.86	5.17	6.84	6.93	7.73	7.99	8.14	6.79	6.88	7.66	7.90	8.06	6.74	6.81	7.26	7.76	7.91
C240-T1.0-D0.7B2.5	20.86	1.87	3.10	3.25	3.63	3.74	3.76	3.08	3.24	3.57	3.69	3.72	3.04	3.21	3.51	3.63	3.65
C240-T1.0-D0.1B3.0	20.86	19.08	19.57	19.6	19.71	19.77	19.86	19.52	19.54	19.66	19.71	19.82	19.45	19.47	19.57	19.64	19.78
C240-T1.0-D0.3B3.0	20.86	9.96	12.11	12.26	13.05	13.28	13.38	12.02	12.25	12.89	13.11	13.32	11.82	12.16	12.47	12.95	13.12
C240-T1.0-D0.5B3.0	20.86	4.11	5.87	5.96	6.57	6.82	6.97	5.87	5.96	6.51	6.82	6.95	5.73	5.91	6.34	6.69	6.84
C240-T1.5-D0.1B2.0	35.98	35.28	35.96	36.00	36.06	36.15	36.25	35.82	35.96	36.03	36.13	36.23	35.77	35.91	35.94	36.05	36.08
C240-T1.5-D0.3B2.0	35.98	21.97	26.64	26.74	28.52	29.16	29.35	26.6	26.65	28.29	28.82	29.14	26.55	26.56	27.40	28.51	28.82
C240-T1.5-D0.5B2.0	35.98	11.28	14.92	15.19	17.05	17.74	18.16	14.89	14.61	16.78	17.66	18.08	14.88	14.57	16.18	17.4	17.78
C240-T1.5-D0.7B2.0	35.98	4.38	7.84	8.17	8.36	8.53	8.76	7.73	8.09	8.28	8.51	8.76	7.68	8.05	8.19	8.44	8.67
C240-T1.5-D0.1B2.5	35.98	33.28	35.56	35.62	35.65	35.66	35.67	35.49	35.57	35.58	35.62	35.62	35.43	35.48	35.54	35.56	35.57
C240-T1.5-D0.3B2.5	35.98	19.59	23.90	24.03	25.66	26.20	26.49	23.79	23.84	25.38	25.89	26.28	23.69	23.71	24.56	25.58	25.97
C240-T1.5-D0.5B2.5	35.98	9.74	12.75	12.83	14.21	14.79	15.23	12.66	12.74	14.09	14.61	15.09	12.56	12.61	13.35	14.35	14.81
C240-T1.5-D0.7B2.5	35.98	3.37	6.12	6.28	6.37	6.41	6.52	6.07	6.25	6.21	6.35	6.48	5.98	6.20	6.10	6.25	6.36
C240-T1.5-D0.1B3.0	35.98	32.20	35.09	35.13	35.16	35.2	35.21	34.99	35.03	35.08	35.12	35.13	34.84	34.87	34.95	34.99	35.11
C240-T1.5-D0.3B3.0	35.98	17.44	21.39	21.56	23.11	23.64	23.85	21.22	21.54	22.83	23.34	23.74	20.86	21.37	22.09	23.05	23.4
C240-T1.5-D0.5B3.0	35.98	7.42	10.51	10.63	12.11	12.55	12.96	10.5	10.62	12.01	12.54	12.92	10.25	10.54	11.69	12.3	12.71
C240-T2.0-D0.1B2.0	54.74	50.91	51.83	52.00	52.02	52.11	52.19	51.64	51.95	51.98	52.07	52.16	51.53	51.84	51.87	52.00	52.12
C240-T2.0-D0.3B2.0	54.74	32.93	40.70	40.92	43.76	44.75	45.34	40.62	40.78	43.42	44.23	45.01	40.49	40.75	42.05	43.75	44.52
C240-T2.0-D0.5B2.0	54.74	16.62	23.14	23.93	27.30	28.32	29.22	23.05	23.57	26.87	28.19	29.09	22.92	23.37	25.91	27.77	28.61
C240-T2.0-D0.7B2.0	54.74	6.93	11.43	12.09	12.56	12.6	12.74	11.28	11.98	12.45	12.57	12.70	11.14	11.86	12.26	12.52	12.66
C240-T2.0-D0.1B2.5	54.74	50.55	53.17	53.35	53.51	53.67	53.87	53.07	53.27	53.41	53.60	53.79	52.98	53.17	53.32	53.53	53.69
C240-T2.0-D0.3B2.5	54.74	29.15	36.23	36.51	39.12	40.10	40.76	36.06	36.23	38.84	39.83	40.36	35.72	36.01	38.13	39.55	40.12
C240-T2.0-D0.5B2.5	54.74	13.30	19.39	19.81	22.44	22.89	23.30	19.25	19.67	22.17	22.72	23.01	19.04	19.60	21.09	22.35	22.66
C240-T2.0-D0.7B2.5	54.74	5.23	7.97	8.46	8.86	9.00	9.11	7.91	8.44	8.63	8.91	9.05	7.86	8.43	8.54	8.85	8.99
C240-T2.0-D0.1B3.0	54.74	49.97	52.94	53.11	53.14	53.17	53.21	52.92	53.08	53.10	53.13	53.16	52.54	52.76	52.87	52.99	53.10
C240-T2.0-D0.3B3.0	54.74	25.76	32.23	32.56	34.94	35.85	36.43	32.06	32.27	34.62	35.44	36.34	31.87	31.99	33.86	35.18	35.88
C240-T2.0-D0.5B3.0	54.74	10.96	16.31	16.61	18.69	18.89	19.13	16.1	16.47	18.58	18.86	19.12	16.00	16.41	17.70	18.44	18.85

Table 4b Shear strength obtained from the parametric study for section C240 with yield strength (f_y) of 450 MPa

Specimen	Plain web	Unstiffened elongated web holes	Shear strength results of edge-stiffened elongated web holes from FEA, V_{FEA} (kN)														
			R_q=2					R_q=4					R_q=6				
			Q0.04	Q0.06	Q0.08	Q0.10	Q0.12	Q0.04	Q0.06	Q0.08	Q0.10	Q0.12	Q0.04	Q0.06	Q0.08	Q0.10	Q0.12
	(kN)	(kN)	(mm)	(mm)	(mm)	(mm)	(mm)	(mm)	(mm)	(mm)	(mm)	(mm)	(mm)	(mm)	(mm)	(mm)	(mm)
C240-T1.0-D0.1B2.0	29.13	27.48	28.13	28.24	28.37	28.42	28.60	28.10	28.18	28.30	28.37	28.51	28.06	28.14	28.21	28.31	28.39
C240-T1.0-D0.3B2.0	29.13	16.65	20.58	20.65	21.76	22.07	22.17	20.53	20.58	20.21	20.60	20.69	20.45	20.53	19.45	20.18	20.28
C240-T1.0-D0.5B2.0	29.13	9.10	11.57	11.64	12.85	13.26	13.49	11.54	11.61	12.66	13.03	13.39	11.49	11.58	11.96	12.82	13.17
C240-T1.0-D0.7B2.0	29.13	3.55	5.35	5.53	5.63	5.79	5.86	5.31	5.50	5.58	5.74	5.82	5.29	5.45	5.53	5.69	5.77
C240-T1.0-D0.1B2.5	29.13	26.8	27.38	27.48	27.53	27.56	27.63	27.30	27.36	27.1	27.51	27.57	27.26	27.29	26.16	27.37	27.53
C240-T1.0-D0.3B2.5	29.13	15.33	18.82	18.97	19.93	20.29	20.40	18.73	18.82	19.71	20.06	20.23	18.65	18.72	19.08	19.82	20.00
C240-T1.0-D0.5B2.5	29.13	7.55	10.14	10.29	10.80	11.13	11.45	10.07	10.22	10.70	11.00	11.34	9.99	10.11	10.14	10.80	11.13
C240-T1.0-D0.7B2.5	29.13	2.76	4.19	4.36	4.46	4.60	4.69	4.12	4.32	4.42	4.55	4.64	4.09	4.28	4.39	4.51	4.60
C240-T1.0-D0.1B3.0	29.13	26.58	27.15	27.19	27.34	27.43	27.55	27.07	27.11	27.27	27.33	27.49	26.98	27.01	27.15	27.25	27.44
C240-T1.0-D0.3B3.0	29.13	13.87	17.48	17.53	18.32	18.67	18.81	17.34	17.53	18.1	18.43	18.72	17.05	17.47	17.51	18.21	18.46
C240-T1.0-D0.5B3.0	29.13	6.12	8.70	8.77	9.33	9.65	9.91	8.34	8.53	9.10	9.43	9.88	8.05	8.27	8.81	9.21	9.72
C240-T1.5-D0.1B2.0	48.56	48.24	49.54	49.59	49.69	49.81	49.94	49.35	49.55	49.64	49.77	49.91	49.28	49.47	49.51	49.67	49.70
C240-T1.5-D0.3B2.0	48.56	29.84	36.61	36.75	39.19	40.07	40.33	36.55	36.62	38.88	39.60	40.04	36.49	36.5	37.66	39.18	39.60
C240-T1.5-D0.5B2.0	48.56	15.70	20.75	21.18	23.22	24.14	24.74	20.71	20.38	22.85	24.03	24.62	20.69	20.32	22.03	23.68	24.22
C240-T1.5-D0.7B2.0	48.56	6.00	11.05	11.50	11.88	12.10	12.49	10.90	11.39	11.78	12.07	12.49	10.82	11.33	11.65	11.97	12.37
C240-T1.5-D0.1B2.5	48.56	45.27	48.7	48.79	48.83	48.85	48.85	48.61	48.72	48.74	48.79	48.78	48.52	48.6	48.67	48.71	48.72
C240-T1.5-D0.3B2.5	48.56	26.91	33.13	33.26	35.35	36.09	36.44	32.98	33.00	34.96	35.67	36.14	32.83	32.82	33.83	35.24	35.72
C240-T1.5-D0.5B2.5	48.56	12.67	17.16	17.44	19.29	20.05	20.65	17.04	17.31	19.12	19.81	20.46	16.91	17.14	18.11	19.46	20.08
C240-T1.5-D0.7B2.5	48.56	4.68	7.90	8.10	8.22	8.28	8.42	7.84	8.07	8.01	8.19	8.36	7.72	8.00	7.87	8.06	8.20
C240-T1.5-D0.1B3.0	48.56	43.63	48.05	48.10	48.15	48.21	48.22	47.92	47.98	48.04	48.09	48.11	47.72	47.75	47.86	47.92	48.08
C240-T1.5-D0.3B3.0	48.56	24.03	29.98	30.05	32.14	32.87	33.20	29.75	30.03	31.75	32.45	33.04	29.25	29.8	30.71	32.06	32.57
C240-T1.5-D0.5B3.0	48.56	10.61	14.15	14.47	16.39	17.05	17.53	14.13	14.47	16.25	17.03	17.48	13.79	14.35	15.82	16.70	17.20
C240-T2.0-D0.1B2.0	73.58	71.94	73.87	73.96	74.09	74.28	74.48	73.6	73.89	74.03	74.23	74.43	73.49	73.77	73.83	74.07	74.12
C240-T2.0-D0.3B2.0	73.58	44.99	55.76	55.81	59.46	60.66	61.43	55.66	55.63	59.00	59.96	61.00	55.57	55.44	57.14	59.32	60.32
C240-T2.0-D0.5B2.0	73.58	23.23	31.61	31.99	35.71	37.26	38.49	31.55	30.77	35.15	37.09	38.31	31.52	30.69	33.89	36.54	37.69
C240-T2.0-D0.7B2.0	73.58	8.89	15.27	16.91	17.31	17.50	17.86	15.1	16.88	17.26	17.49	17.83	14.98	16.79	17.04	17.42	17.76
C240-T2.0-D0.1B2.5	73.58	71.42	73.59	73.72	73.78	73.81	73.82	73.45	73.61	73.64	73.72	73.71	73.32	73.43	73.54	73.60	73.61
C240-T2.0-D0.3B2.5	73.58	39.94	50.01	50.15	53.54	54.78	55.56	49.78	49.76	52.95	54.14	55.11	49.56	49.48	51.23	53.49	54.46
C240-T2.0-D0.5B2.5	73.58	18.65	26.28	26.84	29.60	30.97	32.11	26.09	26.65	29.33	30.60	31.81	25.89	26.37	27.79	30.06	31.22
C240-T2.0-D0.7B2.5	73.58	6.51	11.79	12.52	13.25	13.42	13.62	11.72	12.48	13.02	13.35	13.55	11.68	12.46	12.93	13.29	13.48
C240-T2.0-D0.1B3.0	73.58	70.70	72.73	72.81	72.89	72.96	72.99	72.53	72.61	72.71	72.79	72.82	72.22	72.28	72.44	72.53	72.77
C240-T2.0-D0.3B3.0	73.58	35.63	44.95	45.06	48.19	49.37	50.16	44.6	45.02	47.61	48.74	49.93	43.85	44.68	46.06	48.14	49.21
C240-T2.0-D0.5B3.0	73.58	15.32	22.29	22.87	25.44	26.59	27.50	22.26	22.86	25.23	26.56	27.41	21.73	22.67	24.56	26.05	26.97

Table 3c Shear strength obtained from the parametric study for section C290 with yield strength (f_y) of 300 MPa

Specimen	Plain web	Unstiffened elongated web holes	Shear strength results of edge-stiffened elongated web holes from FEA, V_{FEA} (kN)														
			R_q=2					R_q=4					R_q=6				
			Q0.04	Q0.06	Q0.08	Q0.10	Q0.12	Q0.04	Q0.06	Q0.08	Q0.04	Q0.12	Q0.04	Q0.06	Q0.04	Q0.10	Q0.12
	(kN)	(kN)	(mm)	(mm)	(mm)	(mm)	(mm)	(mm)	(mm)	(mm)	(mm)	(mm)	(mm)	(mm)	(mm)	(mm)	(mm)
C290-T1.0-D0.1B2.0	21.60	20.26	22.12	22.14	22.18	22.24	22.30	22.03	22.12	22.17	22.22	22.28	22.00	22.09	22.11	22.18	22.19
C290-T1.0-D0.3B2.0	21.60	13.19	15.90	16.69	17.01	17.15	17.34	15.72	16.14	16.9	17.02	17.22	15.49	16.04	16.61	16.81	16.96
C290-T1.0-D0.5B2.0	21.60	6.93	8.86	9.67	10.05	10.26	10.44	8.84	9.35	9.98	10.18	10.36	8.83	9.09	9.82	10.06	10.21
C290-T1.0-D0.7B2.0	21.60	2.68	4.11	4.75	4.98	5.15	5.26	4.10	4.51	4.90	5.09	5.17	4.09	4.49	4.85	5.07	5.14
C290-T1.0-D0.1B2.5	21.60	19.94	21.66	21.67	21.68	21.68	21.69	21.64	21.62	21.67	21.67	21.68	21.62	21.57	21.00	21.13	21.65
C290-T1.0-D0.3B2.5	21.60	11.98	14.57	15.29	15.62	15.76	15.95	14.55	14.79	15.52	15.65	15.83	14.52	14.69	15.26	15.45	15.60
C290-T1.0-D0.5B2.5	21.60	5.69	7.58	8.12	8.44	8.67	8.65	7.57	7.85	8.39	8.61	8.58	7.56	7.64	8.24	8.50	8.46
C290-T1.0-D0.7B2.5	21.60	2.01	3.38	3.93	4.17	4.28	4.29	3.38	3.73	4.11	4.23	4.21	3.34	3.72	4.07	4.20	4.19
C290-T1.0-D0.1B3.0	21.60	19.60	21.29	21.67	21.87	22.08	22.40	21.24	21.6	21.83	22.00	20.38	21.17	21.45	21.74	21.94	20.23
C290-T1.0-D0.3B3.0	21.60	10.98	13.28	13.93	14.25	14.41	14.60	13.25	13.47	14.16	14.30	14.50	13.23	13.38	13.92	14.13	14.28
C290-T1.0-D0.5B3.0	21.60	4.83	6.48	7.01	7.30	7.52	7.67	6.47	6.66	7.18	7.44	7.54	6.40	6.64	7.12	7.39	7.49
C290-T1.5-D0.1B2.0	38.85	38.32	39.29	39.33	39.41	39.51	39.61	39.14	39.30	39.37	39.48	39.59	39.09	39.24	39.27	39.40	39.42
C290-T1.5-D0.3B2.0	38.85	23.41	28.66	30.13	30.76	31.14	31.53	28.61	29.14	30.56	30.91	31.30	28.56	28.95	30.05	30.53	30.83
C290-T1.5-D0.5B2.0	38.85	12.05	16.07	17.61	18.43	18.98	19.36	16.04	17.03	18.31	18.84	19.23	16.02	16.55	18.00	18.6	18.94
C290-T1.5-D0.7B2.0	38.85	4.79	8.39	9.24	9.31	9.55	9.69	8.36	8.89	9.29	9.53	9.66	8.25	8.76	9.27	9.50	9.60
C290-T1.5-D0.1B2.5	38.85	37.53	38.73	38.83	38.89	39.07	39.09	38.69	38.73	38.87	38.98	39.03	38.64	38.68	38.75	38.93	38.95
C290-T1.5-D0.3B2.5	38.85	21.02	25.87	27.25	27.92	28.32	28.68	25.82	26.35	27.74	28.11	28.48	25.78	26.18	27.27	27.76	28.05
C290-T1.5-D0.5B2.5	38.85	9.78	13.36	14.48	15.17	15.71	16.07	13.34	14.00	15.07	15.59	15.95	13.31	13.62	14.82	15.4	15.71
C290-T1.5-D0.7B2.5	38.85	3.66	6.45	7.09	7.25	7.34	7.49	6.44	6.74	7.13	7.25	7.36	6.37	6.72	7.07	7.20	7.31
C290-T1.5-D0.1B3.0	38.85	36.95	37.91	37.78	37.99	38.09	38.12	37.57	37.62	37.69	37.70	37.71	37.35	37.38	37.4	37.44	37.48
C290-T1.5-D0.3B3.0	38.85	19.02	23.21	24.51	25.2	25.57	25.96	23.17	23.7	25.04	25.39	25.77	23.13	23.55	24.61	25.07	25.39
C290-T1.5-D0.5B3.0	38.85	8.11	11.41	12.29	12.89	13.38	13.72	11.38	11.68	12.68	13.22	13.48	11.26	11.64	12.58	13.14	13.39
C290-T2.0-D0.1B2.0	58.21	55.22	58.64	58.71	58.82	58.97	59.12	58.42	58.65	58.77	58.92	59.09	58.34	58.56	58.61	58.80	58.84
C290-T2.0-D0.3B2.0	58.21	35.25	43.85	46.04	47.02	47.75	48.41	43.78	44.53	46.72	47.40	48.07	43.70	44.23	45.93	46.81	47.35
C290-T2.0-D0.5B2.0	58.21	17.87	24.72	26.94	28.41	29.54	30.29	24.67	26.06	28.22	29.32	30.08	24.63	25.33	27.75	28.96	29.62
C290-T2.0-D0.7B2.0	58.21	7.15	12.31	13.34	13.62	13.95	14.19	12.25	13.02	13.56	13.85	14.12	12.16	12.89	13.48	13.75	14.06
C290-T2.0-D0.1B2.5	58.21	54.28	58.00	58.06	58.17	58.31	58.47	57.78	58.00	58.12	58.27	58.43	57.69	57.91	57.96	58.15	58.19
C290-T2.0-D0.3B2.5	58.21	31.34	39.16	41.28	42.40	43.11	43.66	39.09	39.92	42.12	42.79	43.35	39.02	39.65	41.41	42.26	42.70
C290-T2.0-D0.5B2.5	58.21	14.40	20.4	22.19	23.44	24.42	25.12	20.37	21.46	23.29	24.24	24.95	20.33	20.86	22.89	23.94	24.57
C290-T2.0-D0.7B2.5	58.21	5.42	9.25	10.30	10.62	10.76	10.84	9.21	9.94	10.57	10.62	10.80	9.20	9.88	10.46	10.58	10.74
C290-T2.0-D0.1B3.0	58.21	53.07	56.61	56.67	56.78	56.92	57.07	56.40	56.62	56.73	56.88	57.04	56.32	56.53	56.58	56.76	56.80
C290-T2.0-D0.3B3.0	58.21	28.09	34.9	36.87	37.99	38.78	39.34	34.84	35.65	37.75	38.50	39.07	34.78	35.42	37.11	38.02	38.48
C290-T2.0-D0.5B3.0	58.21	11.92	17.4	19.04	19.95	20.85	21.44	17.37	18.09	19.63	20.60	21.06	17.18	18.03	19.46	20.46	20.92

Table 3d Shear strength obtained from the parametric study for section C290 with yield strength (f_y) of 450 MPa

Specimen	Plain web	Unstiffened elongated web holes	Shear strength results of edge-stiffened elongated web holes from FEA, V_{FEA} (kN)														
			R_q=2					R_q=4					R_q=6				
			Q0.04	Q0.06	Q0.08	Q0.10	Q0.12	Q0.04	Q0.06	Q0.08	Q0.04	Q0.12	Q0.04	Q0.06	Q0.04	Q0.10	Q0.12
	(kN)	(kN)	(mm)	(mm)	(mm)	(mm)	(mm)	(mm)	(mm)	(mm)	(mm)	(mm)	(mm)	(mm)	(mm)	(mm)	(mm)
C290-T1.0-D0.1B2.0	29.46	28.06	30.14	30.18	30.23	30.31	30.39	30.03	30.15	30.21	30.29	30.37	29.99	30.10	30.13	30.22	30.24
C290-T1.0-D0.3B2.0	29.46	18.39	22.19	23.11	23.54	23.71	23.92	22.15	22.35	23.39	23.54	23.75	22.11	22.20	22.99	23.25	23.40
C290-T1.0-D0.5B2.0	29.46	9.84	12.75	13.41	13.91	14.44	14.8	12.73	12.97	13.82	14.33	14.70	12.71	12.61	13.59	14.15	14.48
C290-T1.0-D0.7B2.0	29.46	3.66	5.57	6.02	6.33	6.79	6.93	5.54	5.80	6.26	6.74	6.84	5.51	5.71	6.23	6.69	6.79
C290-T1.0-D0.1B2.5	29.46	27.62	29.81	29.82	29.83	29.84	29.84	29.77	29.74	29.81	29.81	29.83	29.75	29.68	28.90	29.07	29.79
C290-T1.0-D0.3B2.5	29.46	16.66	20.70	21.43	21.87	22.06	22.26	20.66	20.73	21.73	21.90	22.10	20.63	20.59	21.36	21.63	21.77
C290-T1.0-D0.5B2.5	29.46	8.35	11.31	11.78	12.17	12.63	12.80	11.29	11.40	12.09	12.54	12.71	11.27	11.08	11.89	12.38	12.51
C290-T1.0-D0.7B2.5	29.46	2.93	4.34	4.99	5.29	5.50	5.67	4.33	4.81	5.28	5.49	5.65	4.31	4.59	5.27	5.47	5.63
C290-T1.0-D0.1B3.0	29.46	27.23	29.58	30.10	30.39	30.67	31.12	29.51	30.01	30.33	30.56	28.31	29.41	29.8	30.20	30.47	28.11
C290-T1.0-D0.3B3.0	29.46	15.43	19.06	19.70	20.05	20.36	20.58	19.03	19.05	19.92	20.21	20.43	19.00	18.93	19.58	19.96	20.12
C290-T1.0-D0.5B3.0	29.46	7.08	9.68	10.10	10.41	10.77	10.96	9.66	9.59	10.24	10.64	10.76	9.56	9.56	10.15	10.57	10.70
C290-T1.5-D0.1B2.0	53.93	52.76	54.08	54.14	54.24	54.38	54.53	53.88	54.09	54.20	54.34	54.49	53.80	54.01	54.06	54.23	54.26
C290-T1.5-D0.3B2.0	53.93	32.01	39.46	41.32	42.18	42.76	43.20	39.39	39.96	41.91	42.44	42.90	39.32	39.69	41.20	41.92	42.25
C290-T1.5-D0.5B2.0	53.93	16.81	22.41	24.15	25.21	26.06	26.55	22.37	23.35	25.05	25.87	26.36	22.33	22.71	24.63	25.54	25.97
C290-T1.5-D0.7B2.0	53.93	6.58	10.56	12.40	13.11	13.45	13.55	10.54	11.95	13.09	13.43	13.50	10.43	11.76	13.06	13.50	13.46
C290-T1.5-D0.1B2.5	53.93	51.71	53.37	53.50	53.59	53.83	53.85	53.31	53.37	53.56	53.70	53.77	53.24	53.3	53.40	53.64	53.67
C290-T1.5-D0.3B2.5	53.93	28.95	36.07	37.73	38.61	39.15	39.60	36.00	36.49	38.36	38.87	39.32	35.94	36.24	37.71	38.38	38.73
C290-T1.5-D0.5B2.5	53.93	13.80	19.07	20.19	21.04	21.85	22.35	19.04	19.53	20.91	21.69	22.20	19.01	18.98	20.55	21.42	21.86
C290-T1.5-D0.7B2.5	53.93	5.06	8.55	9.68	10.12	10.34	10.53	8.51	9.33	10.01	10.25	10.39	8.46	9.28	9.96	10.21	10.33
C290-T1.5-D0.1B3.0	53.93	51.01	52.34	52.16	52.45	52.59	52.63	51.86	51.93	52.03	52.05	52.06	51.56	51.60	51.64	51.68	51.74
C290-T1.5-D0.3B3.0	53.93	26.34	32.86	34.25	35.10	35.66	36.11	32.80	33.12	34.87	35.40	35.86	32.74	32.90	34.28	34.96	35.32
C290-T1.5-D0.5B3.0	53.93	11.63	16.23	17.22	17.98	18.74	19.34	16.19	16.36	17.69	18.51	19.00	16.02	16.31	17.54	18.39	18.88
C290-T2.0-D0.1B2.0	78.52	76.99	80.59	80.68	80.83	81.03	81.24	80.28	80.6	80.76	80.97	81.19	80.17	80.47	80.54	80.8	80.85
C290-T2.0-D0.3B2.0	78.52	47.90	60.15	62.88	64.31	65.32	66.22	60.04	60.81	63.90	64.84	65.76	59.94	60.41	62.81	64.04	64.76
C290-T2.0-D0.5B2.0	78.52	24.76	34.04	36.62	38.57	40.10	41.07	33.98	35.41	38.32	39.81	40.78	33.92	34.43	37.67	39.31	40.17
C290-T2.0-D0.7B2.0	78.52	9.86	16.89	18.82	19.27	19.72	20.09	16.8	17.95	19.25	19.66	20.01	16.69	17.88	19.12	19.50	19.92
C290-T2.0-D0.1B2.5	78.52	75.72	79.87	79.96	80.11	80.31	80.52	79.57	79.88	80.04	80.25	80.47	79.45	79.76	79.83	80.08	80.13
C290-T2.0-D0.3B2.5	78.52	43.03	54.30	56.81	58.27	59.36	60.11	54.21	54.94	57.90	58.92	59.69	54.12	54.57	56.92	58.19	58.79
C290-T2.0-D0.5B2.5	78.52	20.22	28.39	30.32	31.81	33.25	34.10	28.33	29.32	31.61	33.01	33.86	28.29	28.51	31.07	32.60	33.35
C290-T2.0-D0.7B2.5	78.52	7.51	12.83	14.43	14.96	15.04	15.34	12.76	14.19	14.88	14.94	15.24	12.55	13.86	14.71	14.85	15.11
C290-T2.0-D0.1B3.0	78.52	74.06	78.59	78.68	78.82	79.02	79.23	78.30	78.60	78.76	78.96	79.18	78.18	78.48	78.55	78.80	78.85
C290-T2.0-D0.3B3.0	78.52	38.82	48.84	51.08	52.58	53.58	54.41	48.75	49.40	52.24	53.19	54.03	48.67	49.07	51.36	52.53	53.21
C290-T2.0-D0.5B3.0	78.52	16.84	24.21	25.86	27.15	28.42	29.19	24.16	24.57	26.72	28.08	28.68	23.9	24.49	26.49	27.9	28.49

5. Current design rules

5.1 AISI [13] and AS/NZS [14] design rules

5.1.1 For plain webs

The design standards of AISI [13] and AS/NZS [14] provide the DSM-based equations for CFS channel sections having plain webs without web stiffeners. The shear strength (V_n) for CFS sections can be calculated using the following equations:

$$V_n = V_y \qquad for\ \lambda_v \leq 0.815 \tag{3}$$

$$V_n = 0.815\sqrt{V_{cr}V_y} \qquad for\ 0.815 < \lambda_v \leq 1.227 \tag{4}$$

$$V_n = V_{cr} \qquad for\ \lambda_v > 1.227 \tag{5}$$

$$V_n = 0.6\, A_w f_y t \tag{6}$$

$$V_{cr} = \frac{\pi^2 E k_v t^3}{12(1-v^2)d_1} \tag{7}$$

Where, V_y = yield shear load, V_{cr} = elastic shear buckling load of the section with plain webs, A_w = area of the web section, E = young's modulus of the elasticity, k_v= shear buckling coefficient for the section with plain webs, v = poisson's ratio.

5.1.2 For unstiffened web holes

The design standards of AISI [13] and AS/NZS [14] provide the shear reduction factor equations to determine the shear strength (V_{nl}) of CFS sections with non-circular web holes, which were adopted from the design equations of Eiler et al. [15]. shear reduction factor equations (Eqs. 9 to 11) are given below:

$$V_{nl} = q_s V_n \tag{8}$$

$$q_s = 1 \qquad for \quad \frac{c}{t} \geq 54 \tag{9}$$

$$q_s = \frac{c}{54t} \qquad for \quad 5 \leq \frac{c}{t} < 54 \tag{10}$$

$$c = \frac{d_1}{2} - \frac{d_w}{2} \qquad for \quad non-circular\ openings \tag{11}$$

$$\frac{d_w}{d_1} < 0.7, \quad \frac{d_w}{\mathrm{t}} \leq 200, \quad 15mm < d_w \leq 150mm$$

Where, V_n = nominal shear strength of section with plain webs, q_s = shear reduction factor, c = factor for non-circular web holes.

5.2 Shear design rules for unstiffened elongated web holes

5.2.1 Wanniarchchi et al. [30]

Wanniarchchi et al. [30] proposed shear reduction factor equations to calculate the shear strength of CFS channel sections with unstiffened elliptical web holes. The design equations considered the parameters d_w, b_w and d_1 to account for the elliptical shape as similar to elongated web hole (see Fig. 2b). However, these equations are limited to the shear span aspect ratio (a) of 1.0 and $d_w/b_w \leq 1.0$.

$$V_{nl} = q_s V_n \qquad for \quad 0 < \frac{d_w}{d_1} \leq 0.85 \tag{12}$$

$$q_s = \left[1 - 0.6\left(\frac{d_w}{d_1}\right)\right] \qquad for \quad 0 < \frac{d_w}{d_1} \leq 0.30 \tag{13}$$

$$q_s = \left[1.215 - 1.316\left(\frac{d_w}{d_1}\right)\right]\left(\frac{d_w}{b_w}\right)^{0.15} \qquad for \quad 0.30 < \frac{d_w}{d_1} \leq 0.70 \tag{14}$$

$$q_s = \left[0.732 - 0.625\left(\frac{d_w}{d_1}\right)\right]\left(\frac{d_w}{b_w}\right)^{0.15} \qquad for \quad 0.70 < \frac{d_w}{d_1} \leq 0.85 \tag{15}$$

$$\frac{d_w}{b_w} \leq 1.0 \qquad for \quad elliptical\ holes \tag{16}$$

5.2.2 DSM-based equations by Pham et al. [19, 27]

Pham et al. [19, 27] proposed DSM-based design equations to determine the shear strength of CFS channel sections having unstiffened elongated web holes (a = 2.0), based on the simplified methodology of the Vierendeel mechanism proposed by Pham et al. [1, 2].

$$V_n = V_{yh} \qquad for\ \lambda_v \leq 0.587 \tag{17}$$

$$V_n = \left[1 - 0.25\left(\frac{V_{crh}}{V_{yh}}\right)^{0.65}\right]\left(\frac{V_{crh}}{V_{yh}}\right)^{0.65} V_{yh} \qquad for\ \lambda_v > 0.587 \tag{18}$$

$$\lambda = \sqrt{\frac{V_{yh}}{V_{crh}}} \tag{19}$$

$$V_{crh} = \frac{\pi^2 E k_v t^3}{12(1-v^2)d_1} \tag{20}$$

Where the shear yield load (V_{yh}) for channels having elongated web holes can be calculated using the equations given next.

$$V_{yh} = V_y = 0.6\, f_y\, d_1\, t \qquad for\ 0 < \frac{d_{w-eq}}{d_1} \leq 0.1 \tag{21}$$

$$V_{yh} = V_y + a_0 V_y \left(\frac{d_{w-eq}}{d_1} - 0.1\right) + a_1 V_y \left(\frac{d_{w-eq}}{d_1} - 0.1\right)^2 + a_2 V_y \left(\frac{d_{w-eq}}{d_1} - 0.1\right)^3 \qquad for\ 0.1 < \frac{d_{w-eq}}{d_1} \tag{22}$$

$$a_0 = -0.173 - 0.9252\frac{d_{w-eq}}{b_{w-eq}} + 0.0524\frac{d_{w-eq}}{b_{w-eq}} \tag{23}$$

$$a_1 = -3.4095 + 0.9922\frac{d_{w-eq}}{b_{w-eq}} - 0.0995\frac{d_{w-eq}}{b_{w-eq}} \tag{24}$$

$$a_2 = 2.684 - 1.084\frac{d_{w-eq}}{b_{w-eq}} + 0.0466\frac{d_{w-eq}}{b_{w-eq}} \tag{25}$$

Where a_0, a_1 and a_2 are the simplified parameters developed by Pham et al. [27] to account the Vierendeel shear load.

For CFS channel sections with unstiffened elongated web holes, the elastic buckling shear load (V_{crh}) can be calculated using the equations proposed by Pham et al. [19, 27], as shown in the equations below:

$$k_{vh} = \alpha_{vh}\, k_{vo} \tag{26}$$

$$k_{vo} = 4.86 + 6.15\left(\frac{d_1}{a}\right) - 3.63\left(\frac{d_{w-eq}}{d_1}\right) - 19.58\left(\frac{d_{w-eq}}{a}\right) + 13.88\left(\frac{{d_{w-eq}}^2}{d_1 \times a}\right) + 0.57\left(\frac{b_f}{d_1}\right) \tag{27}$$

$$\alpha_{vh} = \left[1 - 0.4\left(\frac{d_{w-eq} - b_{w-eq}}{d_1}\right)\right]^2 \tag{28}$$

$$d_{w-eq} = \left(0.003\ \frac{b_w}{d_w} + 0.822\right) d_w \tag{29}$$

$$A_{wh-eq} = 0.865\ A_{wh} \tag{30}$$

$$b_{w-eq} = \frac{A_{wh-eq}}{d_{w-eq}} \tag{31}$$

Where A_h and A_{h-eq} are the areas of actual and equivalent elongated web openings, respectively.

5.3 Shear design rules for CFS channels with edge-stiffened circular web holes

Chen et al. [3] proposed new design equations in the form of shear reduction factor to determine the shear strength of CFS channel sections with edge-stiffened circular web holes. However, these equations were limited to the shear span aspect ratio of 1.0, $0.04 \leq q/d_1 \leq 0.12$ and $d_w/d_1 \leq 0.70$. The design equations for calculating the shear reduction factor are given below:

$$q_s = 1.04 + 0.67\left(\frac{q}{d_1}\right) - 0.59\left(\frac{d_w}{d_1}\right) \qquad for \quad 0.1 < \frac{d_w}{d_1} \leq 0.30 \tag{32}$$

$$q_s = 1.42 + 1.08\left(\frac{q}{d_1}\right) - 1.59\left(\frac{d_w}{d_1}\right) \qquad for \quad 0.1 < \frac{d_w}{d_1} \leq 0.50 \tag{33}$$

$$q_s = 1.72 + 1.18\left(\frac{q}{d_1}\right) - 1.91\left(\frac{d_w}{d_1}\right) \qquad for \quad 0.1 < \frac{d_w}{d_1} \leq 0.70 \tag{34}$$

6. Comparison of design strengths calculated from the available design guidelines with the FEA results

6.1 For unstiffened elongated web holes

The shear reduction factor of CFS channel sections having unstiffened elongated web holes obtained from the FEA results was compared with the strengths determined by the AISI & AS/NZS [13, 14] and Wanniarchchi et al. [30]. From the comparison results (see Table 4), the shear reduction factor obtained from the design equations of AISI & AS/NZS [13,14] and Wanniarchchi et al. [30] was found to be unconservative. Fig. 17 shows the comparison of results obtained from the DSM-based equations proposed by Pham et al. [15, 16] with the FEA results presented herein, for the unstiffened elongated web holes. The comparison results revealed that the nominal shear strength predicted by the DSM-based equations of Pham et al. [19, 27] was conservative. The mean and COV values of the ratio of FEA results to the current design strengths obtained in accordance with available design equations [13-14,18,15-16] are shown in Table 5.

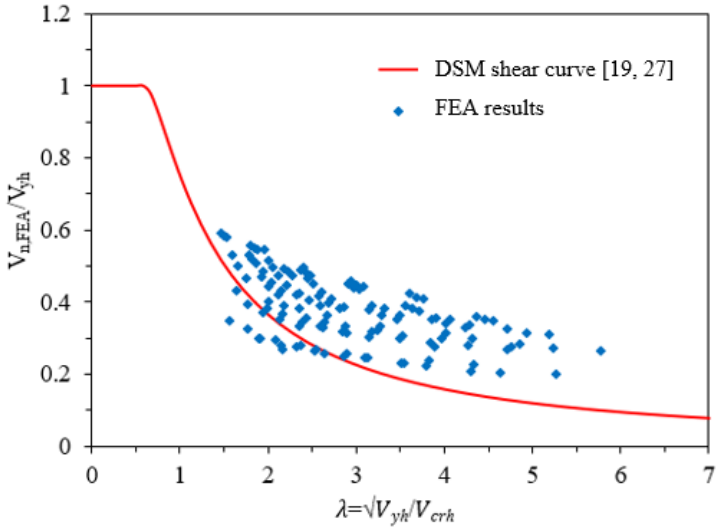

Fig. 17 Comparison of results predicted by the DSM-based equations of Pham et al. [19, 27] with the FEA results for unstiffened web holes

6.2 For edge-stiffened elongated web holes

For CFS channel sections having edge-stiffened elongated web holes, the shear reduction factor equations of sections with edge-stiffened circular web holes proposed by Chen et al. [3] were compared with the FEA results. The comparison results revealed that the design equations proposed by Chen et al. [3] were unconservative (see Table 4). The mean and COV values of the ratio of FEA results to the current design strengths obtained in accordance with Chen et al. [3] are reported in Table 5.

Table 4 Comparison of the shear reduction factors of CFS channel sections with unstiffened and edge-stiffened elongated web holes, obtained from the available design equations

Specimen	Unstiffened elongated web holes					Specimen	Edge-stiffened elongated web holes		
	FEA	AISI & AS/NZS [13, 14]		Wanniarchchi et al. [30]			FEA	Chen et al. [3]	
	$q_{s,FEA}$	$q_{s,[13,14]}$	$q_{s,FEA}/q_{s,[13,14]}$	$q_{s,[30]}$	$q_{s,FEA}/q_{s,[30]}$		$q_{s,FEA}$	$q_{s,[3]}$	$q_{s,FEA}/q_{s,[3]}$
C240-T1.0-D0.1B2.0	0.95	1.00	0.95	0.94	1.01	C240-T2.0-D0.1-B2.0-Q0.04-R2	0.94	1.01	1.00
C240-T1.0-D0.3B2.0	0.58	1.00	0.58	0.82	0.71	C240-T2.0-D0.1-B2.0-Q0.08-R2	0.95	1.03	0.97
C240-T1.0-D0.5B2.0	0.31	1.00	0.31	0.5	0.61	C240-T2.0-D0.1-B2.0-Q0.12-R2	0.95	1.06	0.95
C240-T1.0-D0.7B2.0	0.12	0.67	0.18	0.26	0.44	C240-T2.0-D0.3-B2.0-Q0.04-R2	0.74	0.89	1.13
C240-T1.0-D0.1B2.5	0.92	1.00	0.92	0.94	0.98	C240-T2.0-D0.3-B2.0-Q0.08-R2	0.79	0.92	1.10
C240-T1.0-D0.3B2.5	0.53	1.00	0.53	0.82	0.65	C240-T2.0-D0.3-B2.0-Q0.12-R2	0.82	0.94	1.08
C240-T1.0-D0.5B2.5	0.25	1.00	0.25	0.49	0.51	C240-T2.0-D0.5-B2.0-Q0.04-R2	0.42	0.67	0.97
C240-T1.0-D0.7B2.5	0.09	0.67	0.13	0.26	0.35	C240-T2.0-D0.5-B2.0-Q0.08-R2	0.49	0.71	1.05
C240-T1.0-D0.1B3.0	0.91	1.00	0.91	0.94	0.97	C240-T2.0-D0.5-B2.0-Q0.12-R2	0.53	0.75	1.04
C240-T1.0-D0.3B3.0	0.48	1.00	0.48	0.82	0.58	C240-T2.0-D0.7-B2.0-Q0.04-R2	0.20	0.43	0.86
C240-T1.0-D0.5B3.0	0.20	1.00	0.20	0.47	0.42	C240-T2.0-D0.7-B2.0-Q0.08-R2	0.22	0.48	0.85
C240-T1.5-D0.1B2.0	0.98	1.00	0.98	0.94	1.04	C240-T2.0-D0.7-B2.0-Q0.12-R2	0.23	0.52	0.79
C240-T1.5-D0.3B2.0	0.61	1.00	0.61	0.82	0.74	C240-T2.0-D0.1-B2.5-Q0.04-R2	0.97	1.01	0.98
C240-T1.5-D0.5B2.0	0.31	0.74	0.42	0.50	0.62	C240-T2.0-D0.1-B2.5-Q0.08-R2	0.97	1.03	0.96
C240-T1.5-D0.7B2.0	0.12	0.44	0.27	0.26	0.46	C240-T2.0-D0.1-B2.5-Q0.12-R2	0.98	1.06	0.94
C240-T1.5-D0.1B2.5	0.93	1.00	0.93	0.94	0.98	C240-T2.0-D0.3-B2.5-Q0.04-R2	0.66	0.89	1.01
C240-T1.5-D0.3B2.5	0.54	1.00	0.54	0.82	0.66	C240-T2.0-D0.3-B2.5-Q0.08-R2	0.71	0.92	1.06
C240-T1.5-D0.5B2.5	0.27	0.74	0.37	0.49	0.56	C240-T2.0-D0.3-B2.5-Q0.12-R2	0.74	0.94	1.06
C240-T1.5-D0.7B2.5	0.09	0.44	0.21	0.26	0.37	C240-T2.0-D0.5-B2.5-Q0.04-R2	0.35	0.67	0.82
C240-T1.5-D0.1B3.0	0.89	1.00	0.89	0.94	0.95	C240-T2.0-D0.5-B2.5-Q0.08-R2	0.41	0.71	0.89
C240-T1.5-D0.3B3.0	0.48	1.00	0.48	0.82	0.59	C240-T2.0-D0.5-B2.5-Q0.12-R2	0.42	0.75	0.89
C240-T1.5-D0.5B3.0	0.21	0.74	0.28	0.47	0.44	C240-T2.0-D0.7-B2.5-Q0.04-R2	0.14	0.43	0.64
C240-T2.0-D0.1B2.0	0.93	1.00	0.93	0.94	0.99	C240-T2.0-D0.7-B2.5-Q0.08-R2	0.16	0.48	0.64
C240-T2.0-D0.3B2.0	0.60	0.78	0.77	0.82	0.73	C240-T2.0-D0.7-B2.5-Q0.12-R2	0.16	0.52	0.60
C240-T2.0-D0.5B2.0	0.30	0.56	0.55	0.5	0.61	C240-T2.0-D0.1-B3.0-Q0.04-R2	0.96	1.01	0.99
C240-T2.0-D0.7B2.0	0.13	0.33	0.38	0.26	0.48	C240-T2.0-D0.1-B3.0-Q0.08-R2	0.97	1.03	0.97
C240-T2.0-D0.1B2.5	0.92	1.00	0.92	0.94	0.98	C240-T2.0-D0.1-B3.0-Q0.12-R2	0.97	1.06	0.95
C240-T2.0-D0.3B2.5	0.53	0.78	0.68	0.82	0.65	C240-T2.0-D0.3-B3.0-Q0.04-R2	0.58	0.89	0.93
C240-T2.0-D0.5B2.5	0.24	0.56	0.44	0.49	0.5	C240-T2.0-D0.3-B3.0-Q0.08-R2	0.63	0.92	0.98
C240-T2.0-D0.7B2.5	0.10	0.33	0.29	0.26	0.37	C240-T2.0-D0.3-B3.0-Q0.12-R2	0.66	0.94	0.98
C240-T2.0-D0.1B3.0	0.91	1.00	0.91	0.94	0.97	C240-T2.0-D0.5-B3.0-Q0.04-R2	0.29	0.67	0.71
C240-T2.0-D0.3B3.0	0.47	0.78	0.6	0.82	0.57	C240-T2.0-D0.5-B3.0-Q0.08-R2	0.34	0.71	0.75
C240-T2.0-D0.5B3.0	0.20	0.56	0.36	0.47	0.42	C240-T2.0-D0.5-B3.0-Q0.12-R2	0.35	0.75	0.76

Table 5 Comparison of FEA results with the design strengths determined from the available design standards

Design guidelines	Comparison	Type of web holes	Equations	Mean	COV
AISI & AS/NZS [13, 14]	Shear reduction factor	Unstiffened elongated web holes	Eqs. 8-11	0.54	0.51
Wanniarchchi et al. [30]	Shear reduction factor	Unstiffened elongated web holes	Eqs. 12-16	0.67	0.33
Pham et al. [19, 27]	DSM-based equations	Unstiffened elongated web holes	Eqs. 17-25	0.71	0.32
Chen et al. [3]	Shear reduction factor	Edge-stiffened elongated web holes	Eqs. 32-34	0.70	0.30
Pham et al. [19, 27]	Elastic buckling coefficient	Unstiffened elongated web holes	Eq. 27	0.94	0.17

7. Proposed design equations

7.1 Proposed shear reduction factor equations

The numerical results revealed that the ratios d_w/d_1, b_w/d_w and q/d_1 were the main parameters that affected the shear strength of CFS channels with unstiffened and edge-stiffened elongated web holes. Regression analysis was then carried out to develop new equations for shear reduction factors ($q_{s,Prop}$). The proposed design equations for calculating the shear strength of CFS channels with unstiffened [Eqs. 35 to 37] and edge-stiffened [Eqs. 38 to 40] elongated web holes are given below.

For unstiffened elongated web holes,

$$q_{s,Prop} = 1.38 - 1.99\left(\frac{d_w}{d_1}\right) - 0.09\left(\frac{b_w}{d_w}\right) \qquad for \quad 0 < \frac{d_w}{d_1} \leq 0.30 \tag{35}$$

$$q_{s,prop} = 1.01 - 0.99\left(\frac{d_w}{d_1}\right) - 0.10\left(\frac{b_w}{d_w}\right) \qquad for\ 0.30 < \frac{d_w}{d_1} \leq 0.50 \tag{36}$$

$$q_{s,prop} = 0.47 - 0.33\left(\frac{d_w}{d_1}\right) - 0.06\left(\frac{b_w}{d_w}\right) \qquad for\ 0.50 < \frac{d_w}{d_1} \leq 0.70 \tag{37}$$

For edge-stiffened elongated web holes,

$$q_{s,Prop} = 1.34 + 0.60\left(\frac{q}{d_1}\right) - 1.45\left(\frac{d_w}{d_1}\right) - 0.10\left(\frac{b_w}{d_w}\right) \qquad for \quad 0 < \frac{d_w}{d_1} \leq 0.30 \tag{38}$$

$$q_{s,prop} = 0.31 + 0.87\left(\frac{q}{d_1}\right) + 0.65\left(\frac{d_w}{d_1}\right) - 0.13\left(\frac{b_w}{d_w}\right) \qquad for\ 0.30 < \frac{d_w}{d_1} \leq 0.50 \tag{39}$$

$$q_{s,prop} = 1.15 + 0.38\left(\frac{q}{d_1}\right) - 1.06\left(\frac{d_w}{d_1}\right) - 0.10\left(\frac{b_w}{d_w}\right) \qquad for\ 0.50 < \frac{d_w}{d_1} \leq 0.70 \tag{40}$$

Fig. 18 shows the comparison of the shear reduction factors obtained from the FEA with the ones determined from the proposed equations. It can be seen that the proposed design equations are in good agreement with the FE results in calculating the shear reduction factors (see Table 8). The mean and COV values for FEA over the proposed design equations for unstiffened and edge-stiffened elongated web holes are presented in Tables 6 and 7, respectively. The proposed shear reduction factor equations were limited to $0< d_w/d_1 \leq 0.70$, $2.00 \leq b_w/d_w \leq 3.00$, $0.04 \leq q/d_1 \leq 0.12$.

Table 6 Reliability analysis results of proposed shear reduction factor equations for CFS channel sections with unstiffened elongated web holes

	Proposed shear reduction factor equations		
	Eq. 35	Eq. 36	Eq. 37
Number of data	72	36	24
Mean, P_m	1.00	1.00	1.00
Coefficient of variation, Vp	0.03	0.04	0.03
Reliability index, β	2.82	2.79	2.82
Resistance factor, φ	0.85	0.85	0.85

Table 7 Reliability analysis results of proposed shear reduction factor equations for CFS channel sections with edge-stiffened elongated web holes

	Proposed shear reduction factor equations		
	Eq. 38	Eq. 39	Eq. 40
Number of data	1080	540	360
Mean, P_m	1.00	1.00	1.00
Coefficient of variation, Vp	0.04	0.04	0.07
Reliability index, β	2.80	2.80	2.74
Resistance factor, φ	0.85	0.85	0.85

Table 8 Comparison of the shear reduction factors of CFS channel sections with unstiffened and edge-stiffened elongated web holes, obtained from the proposed equations

Specimen	Unstiffened elongated web holes			Specimen	Edge-stiffened elongated web holes		
	FEA	Proposed equations [Eqs. 35 to 37]			FEA	Proposed equations [Eqs. 38 to 40]	
	$q_{s,FEA}$	$q_{s,Prop}$	$q_{s,Prop}$		$q_{s,FEA}$	$q_{s,Prop}$	$q_{s,FEA}/q_{s,Prop}$
C240-T1.0-D0.1B2.0	0.95	0.99	0.95	C240-T2.0-D0.1-B2.0-Q0.04-R2	0.95	1.02	0.93
C240-T1.0-D0.3B2.0	0.58	0.59	0.98	C240-T2.0-D0.1-B2.0-Q0.08-R2	0.95	1.04	0.91
C240-T1.0-D0.5B2.0	0.31	0.31	0.98	C240-T2.0-D0.1-B2.0-Q0.12-R2	0.95	1.07	0.89
C240-T1.0-D0.7B2.0	0.12	0.12	0.95	C240-T2.0-D0.3-B2.0-Q0.04-R2	0.74	0.73	1.02
C240-T1.0-D0.1B2.5	0.92	0.94	0.97	C240-T2.0-D0.3-B2.0-Q0.08-R2	0.80	0.75	1.06
C240-T1.0-D0.3B2.5	0.53	0.54	0.97	C240-T2.0-D0.3-B2.0-Q0.12-R2	0.83	0.78	1.07
C240-T1.0-D0.5B2.5	0.25	0.26	0.94	C240-T2.0-D0.5-B2.0-Q0.04-R2	0.42	0.42	1.01
C240-T1.0-D0.7B2.5	0.09	0.09	0.95	C240-T2.0-D0.5-B2.0-Q0.08-R2	0.50	0.45	1.10
C240-T1.0-D0.1B3.0	0.91	0.89	1.02	C240-T2.0-D0.5-B2.0-Q0.12-R2	0.53	0.49	1.09
C240-T1.0-D0.3B3.0	0.48	0.49	0.96	C240-T2.0-D0.7-B2.0-Q0.04-R2	0.21	0.21	1.00
C240-T1.0-D0.5B3.0	0.20	0.21	0.93	C240-T2.0-D0.7-B2.0-Q0.08-R2	0.23	0.22	1.02
C240-T1.5-D0.1B2.0	0.98	0.99	0.98	C240-T2.0-D0.7-B2.0-Q0.12-R2	0.23	0.24	0.97
C240-T1.5-D0.3B2.0	0.61	0.59	1.03	C240-T2.0-D0.1-B2.5-Q0.04-R2	0.97	0.97	1.00
C240-T1.5-D0.5B2.0	0.31	0.31	1.00	C240-T2.0-D0.1-B2.5-Q0.08-R2	0.98	0.99	0.98
C240-T1.5-D0.7B2.0	0.12	0.12	0.98	C240-T2.0-D0.1-B2.5-Q0.12-R2	0.98	1.02	0.97
C240-T1.5-D0.1B2.5	0.93	0.94	0.98	C240-T2.0-D0.3-B2.5-Q0.04-R2	0.66	0.68	0.98
C240-T1.5-D0.3B2.5	0.54	0.54	1.00	C240-T2.0-D0.3-B2.5-Q0.08-R2	0.71	0.70	1.02
C240-T1.5-D0.5B2.5	0.27	0.26	1.03	C240-T2.0-D0.3-B2.5-Q0.12-R2	0.74	0.73	1.03
C240-T1.5-D0.7B2.5	0.09	0.09	0.99	C240-T2.0-D0.5-B2.5-Q0.04-R2	0.35	0.35	1.00
C240-T1.5-D0.1B3.0	0.89	0.89	0.99	C240-T2.0-D0.5-B2.5-Q0.08-R2	0.41	0.39	1.05
C240-T1.5-D0.3B3.0	0.48	0.49	0.97	C240-T2.0-D0.5-B2.5-Q0.12-R2	0.43	0.42	1.00
C240-T1.5-D0.5B3.0	0.21	0.21	0.97	C240-T2.0-D0.7-B2.5-Q0.04-R2	0.15	0.16	0.93
C240-T2.0-D0.1B2.0	0.93	0.99	0.93	C240-T2.0-D0.7-B2.5-Q0.08-R2	0.16	0.17	0.94
C240-T2.0-D0.3B2.0	0.60	0.59	1.01	C240-T2.0-D0.7-B2.5-Q0.12-R2	0.17	0.19	0.89
C240-T2.0-D0.5B2.0	0.30	0.31	0.97	C240-T2.0-D0.1-B3.0-Q0.04-R2	0.97	0.92	1.05
C240-T2.0-D0.7B2.0	0.13	0.12	1.02	C240-T2.0-D0.1-B3.0-Q0.08-R2	0.97	0.94	1.03
C240-T2.0-D0.1B2.5	0.92	0.94	0.97	C240-T2.0-D0.1-B3.0-Q0.12-R2	0.97	0.97	1.01
C240-T2.0-D0.3B2.5	0.53	0.54	0.97	C240-T2.0-D0.3-B3.0-Q0.04-R2	0.59	0.63	0.94
C240-T2.0-D0.5B2.5	0.24	0.26	0.92	C240-T2.0-D0.3-B3.0-Q0.08-R2	0.64	0.65	0.98
C240-T2.0-D0.7B2.5	0.10	0.09	1.01	C240-T2.0-D0.3-B3.0-Q0.12-R2	0.67	0.68	0.98
C240-T2.0-D0.1B3.0	0.91	0.89	1.01	C240-T2.0-D0.5-B3.0-Q0.04-R2	0.30	0.29	1.03
C240-T2.0-D0.3B3.0	0.47	0.49	0.94	C240-T2.0-D0.5-B3.0-Q0.08-R2	0.34	0.33	1.05
C240-T2.0-D0.5B3.0	0.20	0.21	0.95	C240-T2.0-D0.5-B3.0-Q0.12-R2	0.35	0.36	0.97

326

7.2 Proposed DSM-based equations

Modified DSM equations [Eqs. 41-47] were also proposed to determine the nominal shear strength ($V_{v,prop}$) of CFS channels with edge-stiffened and unstiffened elongated web holes based on the design equations of Pham et al. [19, 27]. The yield shear load ($V_{yh,prop}$) can be calculated by the following equations [Eqs. 43 and 44], which are based on cubic fit of data presented as per [Eqs. 45-47].

$$V_{n,prop} = V_{yh} \qquad for\ \lambda_v \leq 0.587 \tag{41}$$

$$V_{n,prop} = \left[1 - 0.29\left(\frac{V_{crh}}{V_{yh}}\right)^{0.29}\right]\left(\frac{V_{crh}}{V_{yh}}\right)^{0.29} V_{yh} \qquad for\ \lambda_v > 0.55 \tag{42}$$

$$V_{yh,prop} = V_y = 0.6\, f_y\, d_1\, t_w \qquad for \quad 0 < \frac{d_{w-eq}}{d_1} \leq 0.1 \tag{43}$$

$$V_{yh,prop} = V_y + a_0 V_y \left(\frac{d_{w-eq}}{d_1} - 0.17\right) + a_1 V_y \left(\frac{d_{w-eq}}{d_1} - 0.17\right)^2 + a_2 V_y \left(\frac{d_{w-eq}}{d_1} - 0.17\right)^3 \qquad for \quad 0.1 < \frac{d_{w-eq}}{d_1} \tag{44}$$

$$a_{0,prop} = 0.46 - 2.51\frac{d_{w-eq}}{b_{w-eq}} + 0.10\frac{d_{w-eq}}{b_{w-eq}} \tag{45}$$

$$a_{1,prop} = -0.37 + 4.30\frac{d_{w-eq}}{b_{w-eq}} + 0.70\frac{d_{w-eq}}{b_{w-eq}} \tag{46}$$

$$a_{2,prop} = 2.92 - 8.41\frac{d_{w-eq}}{b_{w-eq}} + 0.03\frac{d_{w-eq}}{b_{w-eq}} \tag{47}$$

In this study, the elastic buckling loads (V_{crh}) of CFS channel sections were obtained from the linear elastic buckling analysis [1, 2] using ABAQUS [38]. A total of 1,062 FE models were developed and the shear buckling coefficients ($k_{vo,FEA}$) were calculated for the CFS channel sections C240 and C290 using the equations (Eqs. 20 and 26). Table. 9 presents the elastic buckling loads obtained from the FEA for C240 CFS channel sections. The proposed design equations of

Pham et al. [19, 27] for calculating the shear buckling coefficients (k_{vo}) of CFS channels with unstiffened elongated web holes were compared with the FEA results of unstiffened elongated web holes. The comparison of FEA results with the shear buckling coefficients (k_{vo}) predicted from the equations of Pham et al. [19, 27], showed that the design equations of Pham et al. [19, 27] were conservative. The comparison results can be found in Table 5.

Modified shear buckling coefficient ($k_{vo,prop}$) equations for unstiffened [Eq. 48] and edge-stiffened [Eq. 49] elongated web holes were therefore proposed based on the FEA results. The elastic buckling load (V_{crh}) for CFS channel sections can be determined using equations [Eqs. 21, 27-33], where k_{vo} can be replaced by the shear buckling coefficient ($k_{vo,prop}$) calculated from equations Eq. 48 and Eq. 49 for unstiffened and edge-stiffened elongated web holes, respectively. The proposed DSM based equations and shear buckling coefficient equations show good correlations with the FEA results (see Figs. 19 and 20). The comparison results of FEA with the proposed DSM design strengths can be found in Tables 10 and 11.

$$k_{vo,prop} = 0.55 + 1.92\left(\frac{d_1}{\mathrm{a}}\right) - 11.89\left(\frac{d_{w-eq}}{d_1}\right) - 5.44\left(\frac{d_{w-eq}}{\mathrm{a}}\right) + 21.31\left(\frac{{d_{w-eq}}^2}{d_1 \times \mathrm{a}}\right) 35.65\left(\frac{b_f}{d_1}\right) \quad (48)$$

$$k_{vo,prop} = -11.46 + 3.25\left(\frac{d_1}{\mathrm{a}}\right) - 0.68\left(\frac{d_{w-eq}}{d_1}\right) - 15.99\left(\frac{d_{w-eq}}{\mathrm{a}}\right) + 10.58\left(\frac{{d_{wh-eq}}^2}{d_1 \times \mathrm{a}}\right) + 96.32\left(\frac{b_f}{d_1}\right) + 19.95\left(\frac{\mathrm{q}}{\mathrm{a}}\right) + 0.20\left(\frac{b_{w-eq}}{\mathrm{a}}\right) + 11.01\left(\frac{\mathrm{r_q}}{\mathrm{a}}\right) \quad (49)$$

Table 9 Elastic buckling loads obtained from the parametric study for section C240

Specimen	Unstiffened elongated web holes	Elastic buckling load results of edge-stiffened elongated web holes from FEA, V_{crh}														
		R_q=2					R_q=4					R_q=6				
		Q0.04	Q0.06	Q0.08	Q0.10	Q0.12	Q0.04	Q0.06	Q0.08	Q0.10	Q0.12	Q0.04	Q0.06	Q0.08	Q0.10	Q0.12
	V_{crh}	(mm)	(mm)	(mm)	(mm)	(mm)	(mm)	(mm)	(mm)	(mm)	(mm)	(mm)	(mm)	(mm)	(mm)	(mm)
C240-T1.0-D0.1B2.0	3.35	3.80	3.80	3.81	3.82	3.83	3.81	3.82	3.82	3.82	3.83	3.83	3.84	3.84	3.85	3.86
C240-T1.0-D0.3B2.0	2.05	3.54	3.63	3.69	3.74	3.80	3.56	3.64	3.70	3.75	3.80	3.57	3.67	3.72	3.77	3.82
C240-T1.0-D0.5B2.0	1.14	3.09	3.21	3.29	3.35	3.41	3.11	3.23	3.30	3.36	3.41	3.13	3.26	3.33	3.39	3.44
C240-T1.0-D0.7B2.0	0.74	2.80	2.97	3.07	3.14	3.21	2.81	2.97	3.06	3.13	3.19	2.81	2.99	3.08	3.14	3.2
C240-T1.0-D0.1B2.5	3.21	3.79	3.82	3.85	3.85	3.86	3.81	3.84	3.86	3.86	3.87	3.83	3.85	3.88	3.88	3.89
C240-T1.0-D0.3B2.5	1.75	3.27	3.36	3.43	3.49	3.55	3.28	3.38	3.44	3.50	3.55	3.29	3.40	3.47	3.52	3.57
C240-T1.0-D0.5B2.5	0.92	2.64	2.74	2.81	2.87	2.92	2.65	2.76	2.82	2.87	2.92	2.66	2.79	2.85	2.9	2.94
C240-T1.0-D0.7B2.5	0.42	2.19	2.34	2.42	2.48	2.53	2.21	2.35	2.43	2.49	2.54	2.23	2.39	2.47	2.52	2.56
C240-T1.0-D0.1B3.0	3.10	3.78	3.82	3.85	3.88	3.90	3.80	3.83	3.86	3.89	3.91	3.82	3.85	3.88	3.90	3.93
C240-T1.0-D0.3B3.0	1.37	3.00	3.10	3.17	3.24	3.30	3.01	3.11	3.18	3.24	3.30	3.02	3.14	3.20	3.26	3.31
C240-T1.0-D0.5B3.0	0.73	2.16	2.25	2.31	2.35	2.40	2.17	2.26	2.31	2.36	2.40	2.17	2.28	2.33	2.37	2.41
C240-T1.5-D0.1B2.0	10.84	12.26	12.33	12.34	12.35	12.36	12.31	12.37	12.37	12.38	12.85	12.36	12.41	12.42	12.42	12.43
C240-T1.5-D0.3B2.0	6.52	11.38	11.71	11.93	12.13	12.31	11.41	11.75	11.97	12.15	12.33	11.43	11.82	12.04	12.21	12.37
C240-T1.5-D0.5B2.0	3.56	9.69	10.23	10.53	10.75	10.95	9.74	10.28	10.57	10.79	10.98	9.77	10.35	10.66	10.87	11.04
C240-T1.5-D0.7B2.0	2.35	8.59	9.35	9.74	10.01	10.22	8.63	9.36	9.75	10.01	10.22	8.64	9.40	9.80	10.06	10.25
C240-T1.5-D0.1B2.5	10.4	12.24	12.34	12.43	12.47	12.48	12.28	12.38	12.47	12.50	12.51	12.33	12.44	12.51	12.54	12.56
C240-T1.5-D0.3B2.5	5.53	10.46	10.85	11.10	11.32	11.51	10.49	10.89	11.13	11.33	11.52	10.49	10.95	11.20	11.39	11.56
C240-T1.5-D0.5B2.5	2.87	8.16	8.68	8.95	9.15	9.32	8.21	8.72	8.99	9.18	9.35	8.23	8.78	9.06	9.25	9.40
C240-T1.5-D0.7B2.5	1.61	6.61	7.35	7.69	7.92	8.10	6.68	7.41	7.75	7.97	8.15	6.71	7.48	7.84	8.06	8.22
C240-T1.5-D0.1B3.0	10.04	12.19	12.32	12.43	12.51	12.59	12.24	12.36	12.46	12.55	12.63	12.28	12.42	12.51	12.60	12.67
C240-T1.5-D0.3B3.0	4.34	9.56	9.99	10.26	10.49	10.69	9.59	10.02	10.28	10.50	10.69	9.58	10.07	10.34	10.54	10.72
C240-T1.5-D0.5B3.0	2.32	6.69	7.14	7.38	7.55	7.70	6.72	7.17	7.40	7.57	7.71	6.72	7.21	7.46	7.62	7.75
C240-T2.0-D0.1B2.0	24.77	27.92	28.12	28.15	28.16	28.17	28.01	28.20	28.22	28.23	28.24	28.12	28.32	28.32	28.33	28.34
C240-T2.0-D0.3B2.0	14.84	25.77	26.74	27.31	27.77	28.20	25.84	26.82	27.39	27.84	28.26	25.87	26.94	27.53	27.97	28.36
C240-T2.0-D0.5B2.0	7.99	21.40	23.14	23.98	24.56	25.04	21.52	23.23	24.08	24.66	25.13	21.55	23.36	24.24	24.83	25.28
C240-T2.0-D0.7B2.0	5.25	18.26	20.78	21.90	22.62	23.15	18.38	20.84	21.97	22.68	23.22	18.37	20.91	22.08	22.81	23.33
C240-T2.0-D0.1B2.5	23.79	27.86	28.11	28.31	28.47	28.47	27.95	28.20	28.39	28.55	28.57	28.04	28.33	28.50	28.64	28.66
C240-T2.0-D0.3B2.5	12.54	23.61	24.79	25.46	25.98	26.45	23.67	24.86	25.52	26.04	26.49	23.66	24.95	25.65	26.15	26.58
C240-T2.0-D0.5B2.5	6.42	17.82	19.51	20.3	20.83	21.27	17.92	19.60	20.39	20.92	21.34	17.93	19.70	20.53	21.06	21.47
C240-T2.0-D0.7B2.5	3.68	13.68	16.19	17.25	17.89	18.36	13.82	16.33	17.40	18.04	18.51	13.83	16.45	17.58	18.24	18.70
C240-T2.0-D0.1B3.0	22.95	27.75	28.07	28.31	28.51	28.68	27.84	28.16	28.39	28.59	28.77	27.93	28.29	28.51	28.70	28.88
C240-T2.0-D0.3B3.0	9.84	21.50	22.82	23.55	24.11	24.60	21.56	22.88	23.60	24.15	24.62	21.51	22.95	23.71	24.24	24.69
C240-T2.0-D0.5B3.0	5.20	14.52	16.07	16.78	17.24	17.62	14.59	16.13	16.84	17.30	17.67	14.57	16.20	16.94	17.41	17.76

Table 10 Comparison of DSM results of CFS channel sections with unstiffened and edge-stiffened elongated web holes, obtained from the proposed equations

Specimen	Unstiffened elongated web holes			Specimen	Edge-stiffened elongated web holes		
	FEA	Proposed equations [Eqs. 41 to 49]			FEA	Proposed equations [Eqs. 41 to 49]	
	$v_{nl,FEA}/v_{yh,prop}$	$v_{n,prop}/v_{yh,prop}$	$(v_{nl,FEA}/v_{yh,prop})/(v_{n,prop}/v_{yh,prop})$		$v_{nl,FEA}/v_{yh,prop}$	$v_{n,prop}/v_{yh,prop}$	$(v_{nl,FEA}/v_{yh,prop})/(v_{n,prop}/v_{yh,prop})$
C290-T1.0-D0.1B2.0	0.36	0.35	1.01	C290-T2.0-D0.1-B2.0-Q0.04-R2	0.56	0.54	1.03
C290-T1.0-D0.3B2.0	0.33	0.34	0.99	C290-T2.0-D0.1-B2.0-Q0.08-R2	0.56	0.55	1.02
C290-T1.0-D0.5B2.0	0.32	0.34	0.94	C290-T2.0-D0.1-B2.0-Q0.12-R2	0.57	0.56	1.01
C290-T1.0-D0.7B2.0	0.30	0.36	0.83	C290-T2.0-D0.3-B2.0-Q0.04-R2	0.60	0.58	1.03
C290-T1.0-D0.1B2.5	0.35	0.35	1.01	C290-T2.0-D0.3-B2.0-Q0.08-R2	0.64	0.59	1.09
C290-T1.0-D0.3B2.5	0.34	0.33	1.01	C290-T2.0-D0.3-B2.0-Q0.12-R2	0.66	0.59	1.11
C290-T1.0-D0.5B2.5	0.34	0.33	1.03	C290-T2.0-D0.5-B2.0-Q0.04-R2	0.56	0.54	1.02
C290-T1.0-D0.7B2.5	0.31	0.36	0.85	C290-T2.0-D0.5-B2.0-Q0.08-R2	0.56	0.55	1.01
C290-T1.0-D0.1B3.0	0.35	0.35	1.00	C290-T2.0-D0.5-B2.0-Q0.12-R2	0.56	0.56	1.00
C290-T1.0-D0.3B3.0	0.34	0.33	1.05	C290-T2.0-D0.7-B2.0-Q0.04-R2	0.59	0.59	1.01
C290-T1.0-D0.5B3.0	0.33	0.32	1.03	C290-T2.0-D0.7-B2.0-Q0.08-R2	0.64	0.59	1.08
C290-T1.5-D0.1B2.0	0.45	0.43	1.04	C290-T2.0-D0.7-B2.0-Q0.12-R2	0.66	0.60	1.10
C290-T1.5-D0.3B2.0	0.39	0.41	0.94	C290-T2.0-D0.1-B2.5-Q0.04-R2	0.54	0.54	1.00
C290-T1.5-D0.5B2.0	0.36	0.41	0.87	C290-T2.0-D0.1-B2.5-Q0.08-R2	0.54	0.55	0.99
C290-T1.5-D0.7B2.0	0.35	0.42	0.84	C290-T2.0-D0.1-B2.5-Q0.12-R2	0.55	0.56	0.98
C290-T1.5-D0.1B2.5	0.44	0.43	1.03	C290-T2.0-D0.3-B2.5-Q0.04-R2	0.58	0.59	0.98
C290-T1.5-D0.3B2.5	0.39	0.41	0.95	C290-T2.0-D0.3-B2.5-Q0.08-R2	0.64	0.60	1.06
C290-T1.5-D0.5B2.5	0.38	0.41	0.92	C290-T2.0-D0.3-B2.5-Q0.12-R2	0.66	0.60	1.09
C290-T1.5-D0.7B2.5	0.35	0.44	0.81	C290-T2.0-D0.5-B2.5-Q0.04-R2	0.60	0.64	0.93
C290-T1.5-D0.1B3.0	0.43	0.42	1.02	C290-T2.0-D0.5-B2.5-Q0.08-R2	0.69	0.65	1.06
C290-T1.5-D0.3B3.0	0.39	0.40	0.97	C290-T2.0-D0.5-B2.5-Q0.12-R2	0.73	0.66	1.12
C290-T1.5-D0.5B3.0	0.36	0.39	0.92	C290-T2.0-D0.7-B2.5-Q0.04-R2	0.63	0.66	0.95
C290-T2.0-D0.1B2.0	0.49	0.50	0.99	C290-T2.0-D0.7-B2.5-Q0.08-R2	0.72	0.67	1.09
C290-T2.0-D0.3B2.0	0.43	0.47	0.91	C290-T2.0-D0.7-B2.5-Q0.12-R2	0.77	0.67	1.16
C290-T2.0-D0.5B2.0	0.40	0.48	0.84	C290-T2.0-D0.1-B3.0-Q0.04-R2	0.60	0.65	0.92
C290-T2.0-D0.7B2.0	0.40	0.48	0.83	C290-T2.0-D0.1-B3.0-Q0.08-R2	0.69	0.65	1.05
C290-T2.0-D0.1B2.5	0.48	0.49	0.98	C290-T2.0-D0.1-B3.0-Q0.12-R2	0.74	0.66	1.12
C290-T2.0-D0.3B2.5	0.43	0.47	0.92	C290-T2.0-D0.3-B3.0-Q0.04-R2	0.75	0.75	0.99
C290-T2.0-D0.5B2.5	0.42	0.47	0.88	C290-T2.0-D0.3-B3.0-Q0.08-R2	0.83	0.76	1.09
C290-T2.0-D0.7B2.5	0.39	0.47	0.83	C290-T2.0-D0.3-B3.0-Q0.12-R2	0.86	0.76	1.13

352

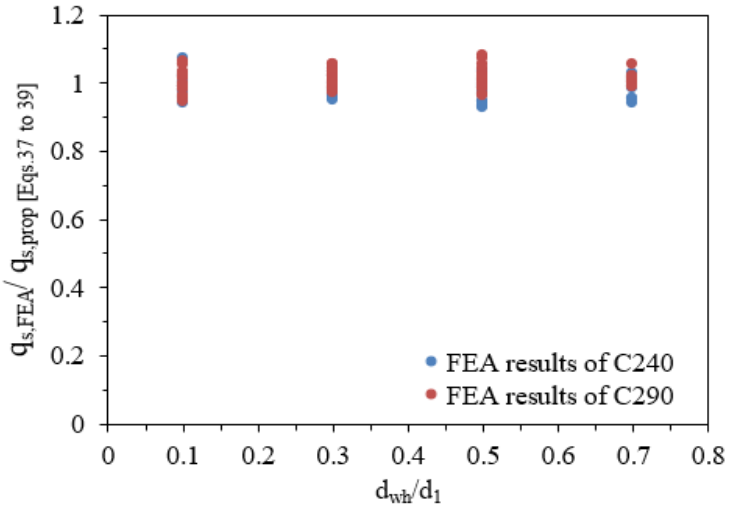

(a) For unstiffened web holes

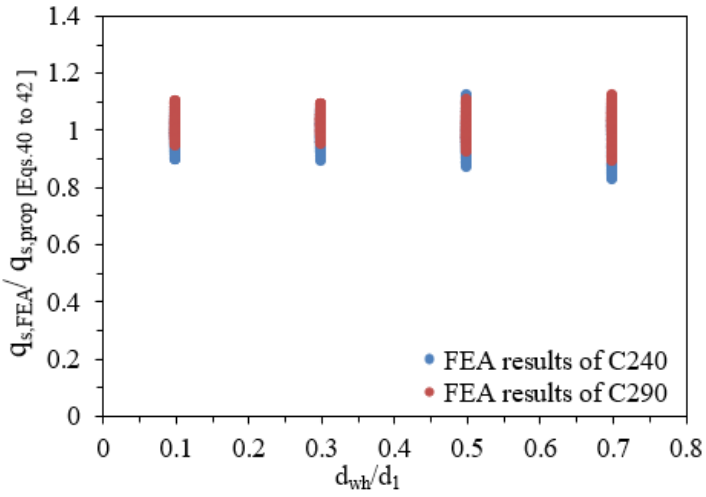

(b) For edge-stiffened web holes

Fig.18 Comparison of shear reduction factors obtained from the FEA with the ones calculated from the proposed equations

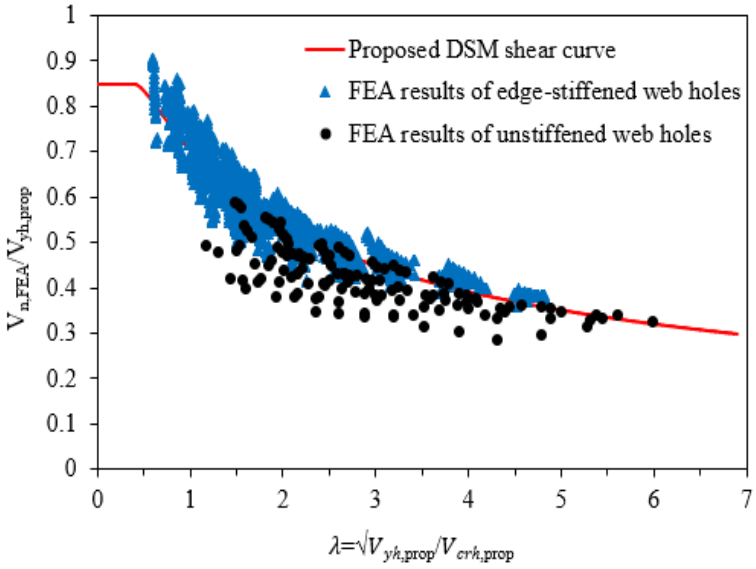

Fig. 19 Comparison of FEA results with the ones calculated from the proposed equations

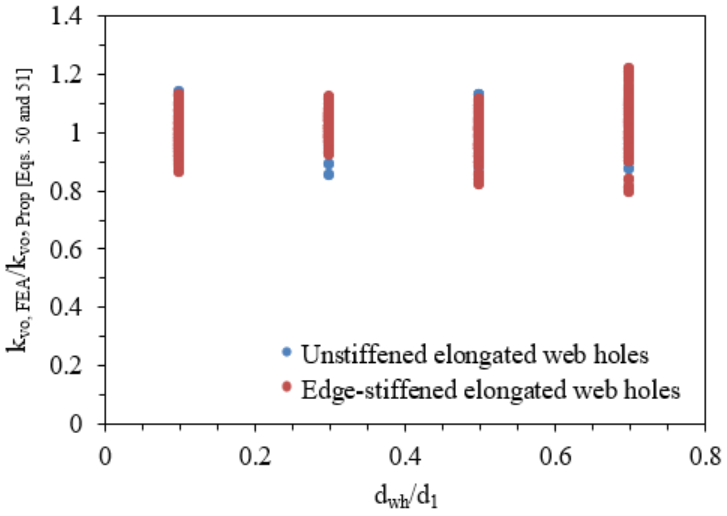

Fig. 20 Comparison of elastic shear buckling coefficient of FEA with the ones calculated from the proposed equations [Eqs. 48 and 49]

Table 11 Reliability analysis results of proposed DSM-based equations for CFS channel sections with edge-stiffened and unstiffened elongated web holes

	Proposed DSM-based equations
	Eqs. 41-49
Number of data	2212
Mean, P_m	1.00
Coefficient of variation, Vp	0.07
Reliability index, β	2.70
Resistance factor, φ	0.85

8. Reliability analysis

A reliability analysis was also conducted to evaluate the accuracy of the proposed design equations of CFS channel sections with unstiffened and edge-stiffened elongated web holes. For CFS structural members, the AISI Specification [13] provides an equation [Eq. 50] and recommends that the lower limit of target reliability index should be 2.5. The design equations are generally considered as reliable if the reliability index (β) value is greater than or equal to 2.5. In this study, the proposed design equations in the form of a shear reduction factor and a DSM-based equations were found to be reliable, while calculating the shear strength of CFS channel sections having unstiffened and edge-stiffened elongated web holes (see Tables 7, 8 and 10).

$$\varphi = 1.52 M_m F_m P_m e^{-\beta \sqrt{\{V_m^2 + V_f^2 + C_p V_p^2 + V_q^2\}}} \tag{50}$$

Where, β = reliability index, φ = resistance factor (0.85), M_m and V_m = mean (1.1) and COV (0.1) of the material factor, F_m and V_f = mean (1.0) and COV (0.05) of the fabrication factor, P_m and V_P = mean and COV of the proposed equation, V_q = COV (0.21) of load effect, C_p = correction factor $\left\lfloor 1 + \frac{1}{n} \right\rfloor \left\lfloor \frac{m}{m-2} \right\rfloor$, n = number of tests and m = degree of freedom (m = n-1).

9. Concluding remarks

This paper presents the results of an extensive numerical investigation on the shear strength of CFS channel sections having unstiffened and edge-stiffened elongated web holes. A total of 2,124 FE models were developed, which include material nonlinearity and initial imperfections. The developed FE models were then validated against the corresponding experimental results reported by Pham et al. (2020b and 2018) and Chen et al. (2022), which showed good agreement in terms of ultimate shear strength, failure behaviour and load-displacement curves. From the parametric study results, the effects of the ratios q/d_1, d_w/d_1, d_w/b_w and R_q on the shear strength of such CFS sections were studied. The following conclusions can be drawn from the outcome of this study:

(1) According to the results of parametric study, the ratios q/d_1, d_w/d_1, and d_w/b_w have a significant influence on the shear reduction factor, while the factor R_q has a negligible effect.

(2) When the parametric results were compared to the design strengths calculated from the design rules specified in the AISI (2016), AS/NZS (2018) and Wanniarchchi et al. (2017) for unstiffened elongated web holes, it showed that these design rules were unconservative. In addition, the direct strength method (DSM) approach equations of Pham et al. (2020a and 2023) showed conservative results for channels with unstiffened elongated web holes. It was also found that the design equations proposed by Chen et al. (2018) for edge-stiffened circular web holes were unconservative, when predicting the shear reduction factor of CFS channels with edge-stiffened elongated web holes.

(3) The design equations for calculating the shear reduction factor of CFS channel sections having unstiffened and edge-stiffened elongated web holes were both proposed based on the linear regression analysis. The limits of the proposed equations were $0.04 \leq q/d_1 \leq 0.12$, $0 < d_w/d_1 \leq$

389 0.70, $2.00 \leq b_w/d_w \leq 3.00$.

390 (4) A comprehensive reliability analysis was then performed, which showed that the proposed
391 equations could be used to accurately calculate the shear reduction factor of CFS channel
392 sections having unstiffened and edge-stiffened elongated web holes.

393 (5) Modified DSM-based design equations were also proposed for CFS channel sections having
394 unstiffened and edge-stiffened web holes, which was shown to be reliable.

395 **References**

396 1. Pham, D. K., Pham, C. H., Pham, S. H., & Hancock, G. J. (2020b). Experimental investigation
397 of high strength cold-formed channel sections in shear with rectangular and slotted web
398 openings. Journal of Constructional Steel Research, 165, 105889.
399 2. Pham, D. K., Pham, C. H., & Hancock, G. J. (2020). Parametric study for shear design of cold-
400 formed channels with elongated web openings. Journal of Constructional Steel Research, 172,
401 106222.
402 3. Chen, B., Roy, K., Fang, Z., Uzzaman, A., Pham, C. H., Raftery, G. M., & Lim, J. B. (2022).
403 Shear capacity of cold-formed steel channels with edge-stiffened web holes, unstiffened web
404 holes, and plain webs. Journal of Structural Engineering, 148(2), 04021268.
405 4. Kanthasamy, E., Thirunavukkarasu, K., Poologanathan, K., Gatheeshgar, P., Todhunter, S.,
406 Suntharalingam, T., & Ishqy, M. F. M. (2022). Shear behaviour of doubly symmetric
407 rectangular hollow flange beam with circular edge-stiffened openings. Engineering
408 Structures, 250, 113366.
409 5. Chen, B., Roy, K., Uzzaman, A., Raftery, G. M., Nash, D., Clifton, G. C., ... & Lim, J. B.
410 (2019). Effects of edge-stiffened web openings on the behaviour of cold-formed steel channel
411 sections under compression. Thin-Walled Structures, 144, 106307.

6. Chen, B., Roy, K., Uzzaman, A., Raftery, G. M., & Lim, J. B. (2020). Parametric study and simplified design equations for cold-formed steel channels with edge-stiffened holes under axial compression. Journal of Constructional Steel Research, 172, 106161.
7. Fang, Z., Roy, K., Chen, B., Sham, C. W., Hajirasouliha, I., & Lim, J. B. (2021). Deep learning-based procedure for structural design of cold-formed steel channel sections with edge-stiffened and un-stiffened holes under axial compression. Thin-Walled Structures, 166, 108076.
8. Yu, C. (2012). Cold-formed steel flexural member with edge stiffened holes: Behaviour, optimization, and design. Journal of Constructional Steel Research, 71, 210-218.
9. Chen, B., Roy, K., Uzzaman, A., & Lim, J. B. (2020). Moment capacity of cold-formed channel beams with edge-stiffened web holes, un-stiffened web holes and plain webs. Thin-Walled Structures, 157, 107070.
10. Dai, Y., Roy, K., Fang, Z., Chen, B., Raftery, G. M., & Lim, J. B. (2022). A novel machine learning model to predict the moment capacity of cold-formed steel channel beams with edge-stiffened and un-stiffened web holes. Journal of Building Engineering, 53, 104592
11. Uzzaman, A., Lim, J. B., Nash, D., & Roy, K. (2020). Cold-formed steel channel sections under end-$_{tw}$o-flange loading condition: Design for edge-stiffened holes, unstiffened holes and plain webs. Thin-Walled Structures, 147, 106532.
12. Chen, B., Roy, K., Fang, Z., Uzzaman, A., Chi, Y., & Lim, J. B. (2021). Web crippling capacity of fastened cold-formed steel channels with edge-stiffened web holes, un-stiffened web holes and plain webs under two-flange loading. Thin-Walled Structures, 163, 107666.
13. AISI (American Iron and Steel Institute). 2016. North American specification for the design of cold-formed steel structural members, 2016 edition. AISI S100-16w. Washington, DC: AISI

14. AS/NZS (Australia/New Zealand Standard). 2018. Cold-formed steel structures. AS/NZS 4600:2018. Sydney, Australia: AS/NZS.
15. Eiler, M. R., LaBoube, R. A., & Yu, W. W. (1997). Behaviour of web elements with openings subjected to linearly varying shear.
16. Keerthan, P., & Mahendran, M. (2013). Experimental studies of the shear behaviour and strength of lipped channel beams with web openings. Thin-Walled Structures, 73, 131-144.
17. Keerthan, P., & Mahendran, M. (2014). Improved shear design rules for lipped channel beams with web openings. Journal of Constructional Steel Research, 97, 127-142.
18. Chandramohan, D. L., Kanthasamy, E., Gatheeshgar, P., Poologanathan, K., Ishqy, M. F. M., Suntharalingam, T., & Kajaharan, T. (2021). Shear behaviour and design of doubly symmetric hollow flange beam with web openings. Journal of Constructional Steel Research, 185, 106836.
19. Pham, D. K., Pham, S. H., Pham, V. B., Pham, C. H., & Hancock, G. J. (2023). Direct Strength Design of Cold-Formed Channels with Web Openings in Shear. Journal of Structural Engineering, 149(4), 04023022.
20. Pham, S. H., Pham, C. H., Rogers, C. A., & Hancock, G. J. (2020). Shear strength experiments and design of cold-formed steel channels with web holes. Journal of Structural Engineering, 146(1), 04019173.
21. Pham, C. H. (2017). Shear buckling of plates and thin-walled channel sections with holes. Journal of Constructional Steel Research, 128, 800-811.
22. Fang, Z., Roy, K., Lakshmanan, D., Pranomrum, P., Li, F., Lau, H. H., & Lim, J. B. (2022). Structural behaviour of back-to-back cold-formed steel channel sections with web openings

under axial compression at elevated temperatures. Journal of Building Engineering, 54, 104512.T

23. Dai, Y., Roy, K., Fang, Z., Chen, B., Raftery, G. M., & Lim, J. B. (2022). A novel machine learning model to predict the moment capacity of cold-formed steel channel beams with edge-stiffened and un-stiffened web holes. Journal of Building Engineering, 53, 104592. T
24. Fang, Z., Roy, K., Liang, H., Poologanathan, K., Ghosh, K., Mohamed, A. M., & Lim, J. B. (2021). Numerical simulation and design recommendations for web crippling strength of cold-formed steel channels with web holes under interior-one-flange loading at elevated temperatures. Buildings, 11(12), 666.
25. Fang, Z., Roy, K., Xu, J., Dai, Y., Paul, B., & Lim, J. B. (2022). A novel machine learning method to investigate the web crippling behaviour of perforated roll-formed aluminium alloy unlipped channels under interior-two flange loading. Journal of Building Engineering, 51, 104261.
26. Fang, Z., Roy, K., Chandramohan, D. L., Yousefi, A., Al-Radhi, Y., & Lim, J. B. (2023). End-One-Flange Web Crippling Behavior of Cold-Formed High-Strength Steel Channels with Web Holes at Elevated Temperatures. Buildings, 13(2), 266.
27. Pham, V. B., Pham, D. K., Pham, S. H., Pham, C. H., & Hancock, G. J. (2020a). Simplification of the Direct Strength Method of Design for Cold-Formed Channels with Holes in Shear. In Proc., Cold-Formed Research Consortium Colloquium. Baltimore: Johns Hopkins Univ.
28. Pham, C. H., & Hancock, G. J. (2020). Shear tests and design of cold-formed steel channels with central square holes. Thin-Walled Structures, 149, 106650.
29. LaBoube, R. A., Yu, W. W., Langan, J. E., & Shan, M. Y. (1997). Cold-formed steel webs with openings: Summary report. Thin-walled structures, 27(1), 79-84.

30. Wanniarachchi, K. S., Mahendran, M., & Keerthan, P. (2017). Shear behaviour and design of Lipped Channel Beams with non-circular web openings. Thin-Walled Structures, 119, 83-102.
31. Sivakumaran, K. S., & Abdel-Rahman, N. (1998). A finite element analysis model for the behaviour of cold-formed steel members. Thin-walled structures, 31(4), 305-324.
32. Moen, C. D., & Schafer, B. W. (2006). Impact of holes on the elastic buckling of cold-formed steel columns.
33. Moen, C. D., & Schafer, B. W. (2008). Experiments on cold-formed steel columns with holes. Thin-Walled Structures, 46(10), 1164-1182.
34. Xu, L., Shi, Y., & Yang, S. (2014). Compressive strength of cold-formed steel c-shape columns with slotted holes.
35. Zhao, J., Liu, S., & Chen, B. (2023). Axial strength of slotted perforated cold-formed steel channels under pinned-pinned boundary conditions. Journal of Constructional Steel Research, 200, 107673.
36. Wang, W., Roy, K., Fang, Z., Ananthi, G.B.G., & Lim, J. B. (2023). Web crippling behaviour of cold-formed steel channel sections having elongated edge-stiffened web holes under interior-two-flange loading condition. Engineering Structures, 294, 116757.
37. Pham, S. H. (2018). Design of cold-formed steel beams with holes and transverse stiffeners in shear (Doctoral thesis). The University of Sydney, Australia.
38. ABAQUS. Analysis User's Manual-Version, ABAQUS INC., USA, 2020.
39. Gardner, L., & Yun, X. (2018). Description of stress-strain curves for cold-formed steels. Construction and Building Materials, 189, 527-538.
40. Rossi, B., Afshan, S., & Gardner, L. (2013). Strength enhancements in cold-formed structural sections—Part II: Predictive models. Journal of Constructional Steel Research, 83, 189-196.

Notations

CFS	Cold-formed steel
FE	Finite element
FEA	Finite element analysis
DSM	Direct strength method
AISI	American Iron and Steel Institute
AS/NZS	Australia/New Zealand Standards
σ	Engineering stress
ε	Engineering strain
E	Young's modulus of elasticity
σ_{true}	True stress
ε_{true}	True strain
d	Depth of the section
t	Thickness of CFS section
f_y	Yield strength
d_w	Depth of web holes
b_w	Length of web holes
b_f	Width of the flange
d_1	Depth of web
l	Length of lip of the section
q	Stiffener length
R_q	Inner bent radius between the web flat and stiffener

q_s	Shear reduction factor
V_y	Yield shear load of cross-section
$q_{s,Prop}$	Proposed shear reduction factor
V_n	Nominal shear strength of section with plain webs
$V_{n,prop}$	Proposed nominal shear strength
V_{cr}	Elastic shear buckling load of section with plain webs
V_{crh}	Elastic shear buckling load of section with web holes
λ_v	Slenderness ratio
A_w	Area of web element
k_v	Shear buckling coefficient
v	Poisson's ratio
V_{nl}	Nominal shear strength of section with web holes
c	Factor for non-circular web holes
V_{yh}	Shear yield load of the section with web holes
$V_{yh,prop}$	Proposed shear yield load of the section with web holes
a_0, a_1, a_2	Simplified parameters to account for the Vierendeel shear load
$a_{0,prop,}\ a_{1,prop},\ a_{2,prop}$	Proposed simplified parameters to account for the Vierendeel shear load
d_{w-eq}	Depth of equivalent elongated holes
b_{w-eq}	Length of equivalent elongated holes
A_{wh-eq}	Area of equivalent elongated holes
A_{wh}	Area of the actual elongated holes
a	Shear span aspect ratio

s	Length of shear span
k_{vh}	Shear buckling coefficient for section with web holes
k_{vo}	Buckling coefficient factor
$k_{vo,prop}$	Proposed buckling coefficient factor
α_{vh}	Factor to account for the elongation level of web holes
V_{EXP}	Shear strength of test
V_{FEA}	Shear strength of parametric study
P_m	Mean value of the proposed equation
V_p	Coefficient of variation of the proposed equation
β	Reliability index
φ	Resistance factor

502